International Journal of Pharmacology

ISSN 1811-7775

science alert

ansinet
Asian Network for Scientific Information

OPEN ACCESS International Journal of Pharmacology

ISSN 1811-7775
DOI: 10.3923/ijp.2024.1247.1270

Research Article
Spectral Analysis of Novel Minocycline/Zn Complex with Promising Anticancer Activities Against Large Lung Cancer Cells (H460), Antibacterial and Antioxidant Activities Against Acrylamide-Induced Pulmonary Toxicity in Male Rats

[1]Samy M. El-Megharbel, [2]Bander Albogami, [3]Shahira A. Hassoubah, [3]Eman A. Beyari, [3]Najah M. Albaqami, [4]Khadeejah Alsolami and [2]Reham Z. Hamza

[1]Department of Chemistry, College of Sciences, Taif University, P.O. Box 11099, Taif 21944, Saudi Arabia
[2]Department of Biology, College of Sciences, Taif University, P.O. Box 11099, Taif 21944, Saudi Arabia
[3]Department of Biological Sciences, Faculty of Science, King Abdulaziz University, Jeddah, Saudi Arabia
[4]Department of Pharmacology and Toxicology, College of Pharmacy, Taif University, P.O. Box 11099, Taif 21944, Saudi Arabia

Abstract

Background and Objective: Minocycline (Mino) is a broad spectrum tetracycline antibiotic, as novel drug complexes attracted attention based on the reduction of possible side effects and producing compounds with new potent capacities, thus the main objective of the study is to assess the potent capacities of new Mino/Zn drug complex. **Materials and Methods:** Minocycline/zinc (Mino/Zn) novel complex was synthesized and characterized using elemental analysis, spectroscopic methods (IR,^{1}H-NMR, UV and X-ray diffraction), magnetic susceptibility, SEM and TEM. An experimental model was used via 32 male rats, divided into 4 groups: Control, Acy, Mino/Zn and Acy plus Mino/Zn. Inflammation markers (CRP, IL-6 and TNF-α), antioxidant enzymes (CAT, SOD and GPx), lipid peroxidation marker (MDA), histological and caspase-3 variations were all investigated in lung tissues, beside estimation of cytotoxicity against large lung cancer cells (H460) and antibacterial activity. **Results:** The non-electrolytic nature of Mino/Zn novel complex was confirmed based on value of molar conductance, Mino is coordinated with Zn metal ion through oxygen atoms of (C = O), ketonic and hydroxyl groups. The surface morphology observed via SEM confirmed that Mino/Zn novel complex appeared as small rectangular projections. The TEM showed formation of black spots for Zn/Mino with particles ranging from 7-19 nm. The Mino/Zn induced highly potent anticancer activities by inhibition of H460 proliferation, the viability of cancer cells was recorded 7.98 µg/mL at concentration of 100 ug/mL. The Mino/Zn alleviated Acy pulmonary toxicity and inflammation markers and has potent antibacterial activities against the bacterial strains (*Bacillus subtilis*, *Staphylococcus aureus* and *Escherichia coli*) at very low concentrations. The Mino/Zn can inhibit viral replication and binding to (ACE2) and the main protease inhibitor M^{pro} receptors via molecular dynamics simulation. **Conclusion:** Novel Mino/Zn novel complex is an effective antioxidant, anticancer and antibacterial agent with cellular inhibitory effect against SARS-CoV-2 via molecular docking simulation.

Key words: Minocycline, minocycline/Zn complex, anticancer activity, lung cancer, oxidative stress

Citation: El-Megharbel, S.M., B. Albogami, S.A. Hassoubah, E.A. Beyari, N.M. Albaqami, K. Alsolami and R.Z. Hamza, 2024. Spectral analysis of novel minocycline/Zn complex with promising anticancer activities against large lung cancer cells (H460), antibacterial and antioxidant activities against acrylamide-induced pulmonary toxicity in male rats. Int. J. Pharmacol., 20: 1247-1270.

Corresponding Author: Samy M. El-Megharbel, Department of Chemistry, College of Sciences, Taif University, P.O. Box 11099, Taif 21944, Saudi Arabia

Funding: This research was funded by Taif University, Saudi Arabia,Project No. (TU-DSPP-2024-155).

Copyright: © 2024 Samy M. El-Megharbel *et al.* This is an open access article distributed under the terms of the creative commons attribution License, which permits unrestricted use, distribution and reproduction in any medium, provided the original author and source are credited.

Competing Interest: The authors have declared that no competing interest exists.

Data Availability: All relevant data are within the paper and its supporting information files.

INTRODUCTION

Minocycline (Mino) is a 2nd-generation, broad-spectrum tetracycline antibiotic. Besides its antibacterial activity, Mino also has anti-inflammatory effects and has the ability to inhibit neuroprotective effects[1,2]. Intra-injection of Mino into septic rats was also shown to improve blood-brain permeability and prognosis[3]. Additionally, Higashida *et al.*[4] found that Mino can inhibit the MMP-9 expression in a rat model of brain injury.

Tetracyclines (TCs) are mainly used as broad-spectrum antibiotics to treat infectious diseases which are caused by pathogens. The TCs bind to the bacterial 30S ribosomal subunit, which results in a great bacteriostatic effect[5]. The intense use and misuse of antibiotics in veterinary medicine have caused widespread bacterial resistance against antibiotics[6].

The Mino was developed to treat atypical and community-acquired infections. Early in 2000, the lack of new antibiotics prompted a reassessment of Mino's efficacy in treating drug-resistant bacteria, including *Stenotrophomonas maltophilia* and *Acinetobacter baumannii*[7-9].

The Mino drew great attention due to its high susceptibility profile, safety profile, good penetration into tissue, high oral bioavailability (making it suitable for step-down therapy) and favorable results from animal and clinical studies[7-9].

The Mino was recently encapsulated with gallium nitrate in nanoparticle nanoformula in niosomes as a drug carrier and used as antibiotic film against *Acinetobacter baumannii* which is considered a worldwide health issue due to its high antibiotic resistance and its high ability to form biofilms. The Mino exhibited great ability against lung toxicity and histological alteration induced by this resistant bacterium[10].

The Mino has anti-inflammatory, immunomodulatory and antioxidant activity besides its anti-bacterial activity. Neuro-protective effects of Mino have also been discovered in many animal models of neurodegeneration injury as Parkinson's and multiple sclerosis[11].

Many evidence from clinical studies has also demonstrated the beneficial effects of Mino on neurodegenerative diseases[12]. The Mino was found to alleviate cognitive impairment by exhibiting both anti-neuro-inflammatory and anti-apoptotic activities[13,14].

The Mino alleviated signs of severe oxidative stress state[15]. Mino has beneficial effects against STZ-induced brain injury[16]. A recent investigation reported the impact of Mino on brain in diabetic rats. Additionally, Mino altered inflammatory cytokines, AChE, antioxidant enzymes such as glutathione and histopathological changes[17-19].

Up-to- date, a few resistances against TCs have been identified, such as the AcrAB/TolC multi-drug pumps[20]. More significantly and importantly, several other studies revealed that Mino attenuated side effects induced by drugs such as (cisplatin, neomycin and gentamycin) hair cell loss (in animal models) and *in vitro* models[21,22].

It is known that Zinc (Zn) metal plays an important role with high affinity in drug–metal complexes. Zinc (Zn) is an essential metal that plays a vital role in reinforcing human immunity. It is an essential element for eliminating the viruses from the host cells. The Zn also, exhibits vital inhibitory effects, against bacterial infections and proliferation of cancer cells, recently zinc oxide nano-spray has exhibited high antiviral activity against SARS-CoV-2 in low concentrations[23].

Lung cancer begins in the lungs and may spread to lymph nodes or other organs in the body. When cancer cells spread from one organ to another, they are called metastases. Lung cancer is the leading cause of cancer-related deaths in the world with non-small cell lung cancer making up about 85% of all lung cancer cases. The H460 cells are a faster-growing cell line, with a growth rate almost double that of small lung cancer cells A549 cells[24-26].

Acrylamide (AC) is a compound formed and present in a lot of foods rich in carbohydrates exposed to a higher temperature during food processing[27]. The ACR is mostly carcinogenic compounds and it induces several types of toxicities in different organs. It has been known that asparagine (amino acid) and reducing sugars in food are the main precursors for ACR production. Due to high consumption and long-term exposure to food rich in carbohydrates, ACR formed in these products could induce genotoxicity and cytotoxicity and may have side effects on human health[28].

This study aimed to assess the anticancer, antibacterial and anti-pulmonary toxicity effect of novel complex of Mino/Zn against lung cancer cell line (A549), bacterial strains (*E. coli*, *S. aureus* and *B. subtilis*) and its ameliorative effect on lung toxicity induced by AC in male rats by evaluation of its chemical and spectroscopic structures and evaluating its activity in inhibition of SARS-CoV-2 via molecular simulation docking.

MATERIALS AND METHODS

Experimental work

Chemicals: All chemicals used: Zinc chloride, ethanol and minocycline hydrochloride are procured from Sigma-Aldrich Chemical Company and were of pure grade as shown in (Fig. 1).

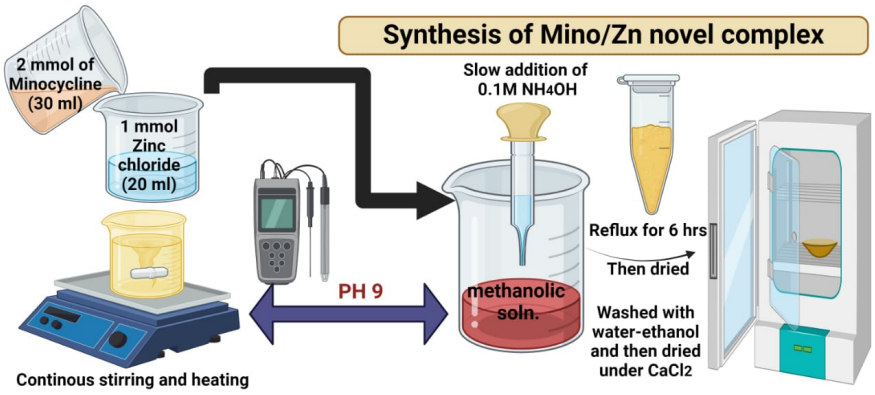

Fig. 1: Synthesis of minocycline/Zn novel complex

Study area: This study was performed in Animal Physiology Lab, based on the Ethical Approval Committee Zu-IACUC: under approval number: ZU-IACUC/1/F/93/2024, for performing the study design and biochemical analysis besides bacterial assessment.

Synthesis of Mino/Zn complex: Solid zinc minocycline compound was prepared by mixing 2 mmol of 30 mL ethanolic solution of minocycline hydrochloride with 1 mmol of 20 mL of distilled water of zinc chloride. Then make refluxing for 6 hrs. White solid product was filtered then washed with a mix of water-ethanol then dried under a vacuum over $CaCl_2$.

Instruments: The IR spectra for minocycline hydrochloride free ligand and its zinc compound were recorded as KBr disks using an IR spectrophotometer at 400-4000 cm^{-1}. Electronic spectra were measured in the range of 800-200 nm using a Spectrophotometer UV2 Unicam UV/Vis. The C, H and N were performed using CHN 2400 PerkinElmer. With DMSO solution of a concentration of 10^{-3} M, conductivity data for zinc minocycline compound was determined using HACH conductivity meter model. Magnetic measurements were measured using Johnson Matthey susceptibility. The ^{1}H-NMR spectra were measured using Bruker AM-500 NMR spectrometer. The SEM images were measured using Joel JSM-6390 equipment. The X-ray diffraction was recorded. The TEM images were measured using JEOL 100s microscopy.

Preparing inoculum (colony suspension method): *Staphylococcus aureus* (ATCC 6538), *Escherichia coli* (ATCC 8739) and *Bacillus subtilis* (ATCC 6633) strains were inoculated into 100 mL of broth medium and the incubation was at 35°C±1.0 for 24 hrs. Except for *Bacillus subtilis* which was incubated at 30°C±1.0 for 24 hrs for preparation of fresh culture agar plate, a loopful from each broth was streaked onto Agar medium and incubated at the previous conditions. A direct sterile 0.1 N NaCl solution was prepared by inoculating 3-4 colonies, suspension was adjusted to achieve turbidity by using Densi CHEK© optical device. Resulting in a suspension containing approximately 1-2×108 CFU/mL[6].

Broth macro-dilution method: Samples in 1 mL Muller Hinton Broth (MHB) were inoculated into all testing wells in 24 wells plate or 12 wells plate. The 2 mL from each sample was inoculated directly in the first well (without dilution), then 1 mL was transferred into the next well, this step was repeated (8 dilutions) for each sample well. After incubation, plates were placed on a dark surface to check the bacterial growth[6].

Antibacterial activity against *Escherichia coli* (ATCC 8739), *Staphylococcus aureus* (ATCC 6538) and *Bacillus subtilis* (ATCC 6633): Discs of *Escherichia coli* (ATCC 8739), *Staphylococcus aureus* (ATCC 6538) and *Bacillus subtilis* (ATCC 6633) both strains were injected into the broth medium and incubated at 30°C for 24 hrs. By using a culture agar plate, a scoop from each broth was streaked very gently into the medium of agar and then incubated at 30°C. The control well, without Mino or its Zn complex, was added to each plate. A (-ve) control well that only contains the broth medium[29]. All the well plates were then incubated at 30°C for only one day. After incubation, the well plates were placed suddenly on the dark surface to concisely check the bacterial growth. All the growth wells produced turbid growth (T) and the (-ve) control wells were very clear without any turbidity which confirmed the validity of this test[30].

Cell culture: Large lung cancer cells (H460) were obtained from Cairo, Egypt. The cells were kept in DMEM media with streptomycin, penicillin and bovine serum in (5% CO_2) atmosphere at (37°C) (Promega Co., USA)[31].

Cytotoxicity assay: Large lung cancer cells (H460) were put in DMEM medium safely with its supplementation. The SRB assay was used to assess the cell viability. A 100 µL of the cell suspensions were seeded in each well plate for one day. After 3 days of exposure to the novel complex Mino/Zn, the cells were fixed by 10% TCA and then washed 3 times with acetic acid instead of the medium that was discarded at 4°C. A German microplate reader called the "BMGLABTECH®-FLUOstar" was used to measure the absorbance at 540 nm[32].

Using MasterPlex 2010 software, the Inhibitory Concentration (IC_{50}) of the cells' viability was ascertained. The IC_{50} values were obtained by plotting the percentage of viable cells. The mean value from the triplicate experiments was obtained and reported as Mean±Standard Deviation. The following equation was used to determine the inhibition percentage (%):

$$\text{Inhibition (\%)} = \frac{\text{Control D} - \text{Sample D}}{\text{Control D}} \times 100$$

where, D is the optical density, (Note: 100% was the control percentage used). The IC_{50} for the novel complex (Mino/Zn) under test, which is the concentration at which 50% of the cells' viability is inhibited or killed.

Molecular docking studies: The current study analyzed the pharmacophoric characteristics of SARS-CoV within ACE2 receptor, co-crystallized (Mino/Zn) using the ligand-based design approach[33]. In order to test the novel formula (Mino/Zn) that binds SARS-CoV-2 via ACE2 receptors.

The referenced tool and study were used[34-36] in predicting the docking and affinity of binding, total fitness and estimated G.

Molecular dynamics simulations were performed for Mino/Zn at 100 nanoseconds using Desmond, a Package of Schrödinger. Molecular docking studies provide a prediction of ligand (Mino) binding state in static conditions. Simulations of the binding status of the novel Mino/Zn complex in the typical physiological environment, simulations were run. The "Maestro" Protein Preparation Wizard was used to preprocess the protein-ligand complex. To determine TIP3P (Transferable Intermolecular Interaction Potential 3 Points), a solvent model featuring an orthorhombic box was chosen. By adding 0.15 M NaCl, the physiological environment should be replicated. To mimic the normal physiological environment via the addition of 0.15 M NaCl. For complete simulation, NPT ensemble with 300 K temperature and 1 atm pressure. The trajectories were saved after every 10 ps for analysis and the stability of simulations was evaluated by calculating the Root Mean Square Deviation (RMSD) of the protein and ligand over time.

Novel complex's physicochemical and pharmacokinetic properties (Mino/Zn): The critical and crucial step in determining the characteristics of the novel Mino/Zn complex is the physicochemical and pharmacokinetic analysis. The novel Mino/Zn complex's physicochemical and pharmacokinetic parameters were assessed using the MD tool[37].

Docking of SARS-CoV-2

ACE2 and M^{pro} receptors with the synthesized novel complex (Mino/Zn): In order to look into the RMSD, scores and L-torsion, the molecular docking step was completed as recommended[38,39].

Molecular dynamics (MD) simulations: The MD simulations for the Mino/Zn novel complex were applied using the Schrödinger package[39-41].

Experimental animals: Based on Zagazig University's Ethical Approval Committee under approval number : ZU-IACUC/1/F/93/2024, the novel complex (Mino/Zn) underwent testing of its biological activity on male rats.

Animal treated groups and animal ethics approval: The ethical approval committee's guidelines were followed with caring for the animals. The 32 male rats weighing 120-150 g and were kept in a typical laboratory setting at 27°C and a regular cycle of daylight. Water and food were available at all times.

The 32 male albino rats were used in the experiment and they were split into 4 treatment groups at random. The rats received the following oral treatments (given via an oral gastric tube) for 30 days in a row:

- **Group (A):** Control group: Received normal physiological saline (0.9 % NaCl)
- **Group (B):** Administrated Acy at a dosage of 500 mg/kg in normal physiological saline solution[42]
- **Group (C):** Given orally Mino/Zn at a dosage of 30 mg/kg and regularly dissolved in the normal saline[43]
- **Group (D):** Given orally Acy and followed by Mino/Zn novel complex after only 30 min, as described for the same doses and treatment duration (Fig. 2)

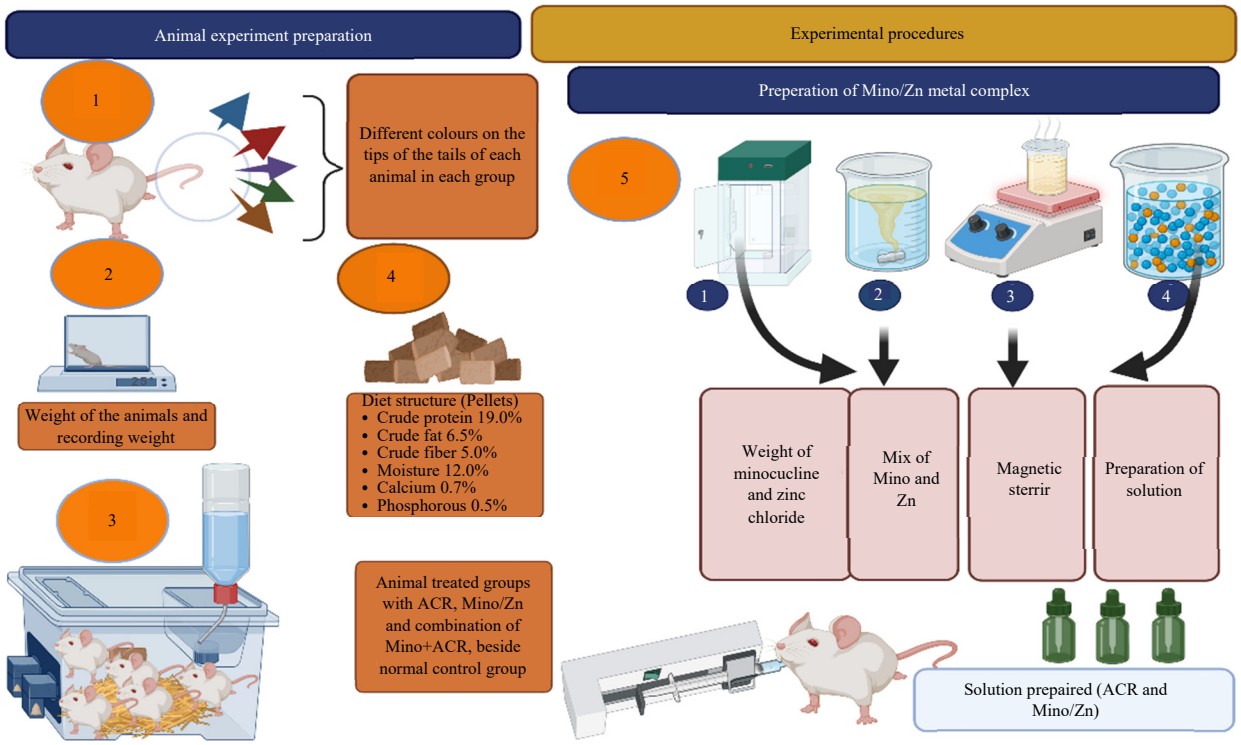

Fig. 2: Graphical representation of the experimental model

Samples collection: To obtain the clear serum, 32 blood samples were centrifuged at 5000 rpm for approximately 15 min. The serum was then stored at -20°C for additional biochemical analysis. Following a brief period of light anesthesia with xylene/ketamine (i.p.), the male rats were abruptly decapitated. The lung tissues were removed and the first part was used for immunological and histological testing. The second part was weighed, homogenized and used to assess the antioxidant enzyme capacities (Fig. 2).

Biochemical markers investigation

Measurement of inflammation markers: The ELISA method was used (Ebio-Science) in accordance with the guidelines to measure Interleukin-6 (IL-6), Tumor Necrosis Factor-Alpha (TNF-α) and C-Reactive Protein (CRP).

Assessment of oxidative stress markers: A 0.25 g sample of the lung tissues was homogenized in a slightly alkaline cold buffer and the supernatant was extracted by centrifugation and utilized for antioxidant assays. Ohkawa *et al.*[44] reported that measurements were made of malondialdehyde (MDA). Superoxide dismutase enzyme activity (SOD) was measured in units of (U/g) in accordance with Marklund and Marklund[45], while CAT activity was estimated in units of (U/g) in accordance with Aebi[46]. Activity of glutathione peroxidase (GPx) was assessed in accordance with manufacturer guidelines[47].

Evaluation of lung tissue histologically and immunohistochemically: The lung tissues were stained with Hematoxylin and Eosin (H&E) for processing of the fixed samples. Using a light microscope (Olympus BX3M upright microscope series and OLYMPUS Stream 2.1 micro-imaging software, UC90 camera, Tokyo, Japan). Photomicrographs of the pulmonary tissues were captured. The extra lung slices (thickness of 4 mm) were stopped. Following the blocking procedure, polyclonal caspase-3 antibody was applied to the tissue sections and left overnight at 4°C. The following color codes were applied to the caspase-3 color intensity in the immunohistochemical sections: (+) for weak immunoreactivity, (++) for moderate immunoreactivity, (+++) for high and strong immunoreactivity and (++++) for extremely high immunoreactivity.

Statistical analysis: The data were reported as Mean±SE and a one-way analysis of variance with *post-hoc* testing was used to compare multiple groups. Significance statistically at $p \leq 0.05$[48]. The assumption was that the GPx in the pulmonary tissue homogenates of the Acy group would be 2.49±0.86 and that of the Acy+Mino/Zn group would be

4.21±0.95 (U/g). Using the OPEN EPI software package, the sample size is 32 (8 in each group) at a power of 80% and a confidence level of 95%[48].

RESULTS AND DISCUSSION

Microanalytical and molar conductance value: The complex zinc minocycline is stable and solid and varies in solubility in common organic solvents but is insoluble in water. The zinc compound's molar conductance value, which indicates its non-electrolytic nature, was measured in 1.0×10^{-3} mol/cm^3 DMSO and found to be Γm = 15 (Ω/mol/cm)[49]. The lack of Cl^- ions outside of the complex sphere is the likely cause of this outcome. The 1:2 zinc:minocycline ratio was verified by the C, H and N analyses as well as the molar conductance data of zinc minocycline $[Zn(Mino)_2]\cdot2H_2O$ as shown in Fig. 3. Elemental analysis, molar conductance, IR, UV, 1H-NMR spectroscopy, TGA/DTG, SEM, TEM and XRD were used to characterize the donation sites for minocycline with Zn(II).

Infrared spectra (FT-IR): The IR for minocycline and its zinc compound are in Fig. 4. For minocycline free ligand and its zinc compound, the IR spectrum showed vibrational bands ranged 3400-2800 cm^{-1} that is attributed to stretching vibrations of (O-H), (N-H) and (C-H) aromatic[50]. With some shifts in wave numbers due to changes in distribution of electronic density for the main attached functional groups and the aromatic rings that occurred after interaction with zinc metal ion. The band appeared for free minocycline at 3350 cm^{-1} assigned to ν (OH) disappeared in zinc complex. The ν (C = O) amide for free minocycline and its zinc complex appeared at the same value at 1649 cm^{-1}, confirming that the carbonyl amide group was not involved in the chelation process. The IR spectrum of minocycline has two bands that appeared at 1754 and 1727 cm^{-1} characterized to (C = O) ketonic rings while for zinc minocycline complex, these two bands are disappeared. It can be concluded that the minocycline compound is coordinated with zinc metal ion through oxygen atoms of (C = O) ketonic and hydroxyl groups. The variation of modes of vibration for C-C, C = C and C-H may change complex formation[51] owing to the newly formed complex's aromaticity differing from the free minocycline. New bands appeared for the zinc complex at 500-550 cm^{-1}, corresponding to ν (M-O) stretching vibration motions[52,53]. Therefore, minocycline acts as a bidentate ligand through the oxygen atoms of ketonic and hydroxyl groups as shown in Fig. 4 as subparts as follows (a) Minocycline and (b) Minocycline/Zn.

UV-Vis spectra: Electronic spectra for minocycline as a free ligand and its zinc compound in solvent "DMSO" are present in Fig. 5 as subparts (a) Minocycline and (b) Minocycline/Zn. By comparing the spectra for Mino and its zinc complexity, it is concluded that Mino has four absorption maxima at 215,230, 250 and 355 nm. The bands that appeared clearly at 215, 230 and 250 nm are assigned to π→π* transitions due to the organic part, while the other band that appeared at 355 nm is assigned to n→π transitions. The zinc (II) complexity shows weak bands at 230, 240, 250 and 350 nm may be assigned to π→π* and n→π* transitions. The magnetic moment for Zn(II)complex is 1.867 BM confirming the square planner configuration of the compound.

^{1}H-NMR spectra: The ^{1}H-NMR spectra for free minocycline and its Zn(II) complex were in DMSO-d6 (Table 1) and Fig. 6(a-b). The spectrum of free minocycline showed a different signal at d (ppm) = (CH, 1.37 and 2.80), (OH alcohol, 4.86), (aromatic benzene ring, 6.80), (OH phenolic, 9.42) and (NH amide,14.85). The H of the NH_2 amide in ^{1}H-NMR spectrum of minocycline and its Zn(II) complex were similar, indicating that NH_2 group remained unaffected after chelation with minocycline. Thus, the NH_2 amide group was not involved in the coordination. The band appeared at 4.16 and 4.38 ppm for zinc complexity assigned to H_2O molecule, which is not present in ^{1}H-NMR spectra of Mino-free ligand.

Thermogravimetric analyses: Thermogravimetric and differential thermogravimetric analysis (TGA-DTG) for Zn^{2+} minocycline complex was performed at 1000°C, which is shown in Fig. 7. It has been noticed that the Zn(II) complexity shows a loss in weight up to 147°C referring to loss of crystalline water and confirm the presence of outside water molecules. The thermal analysis curve for Zn(II) complexity

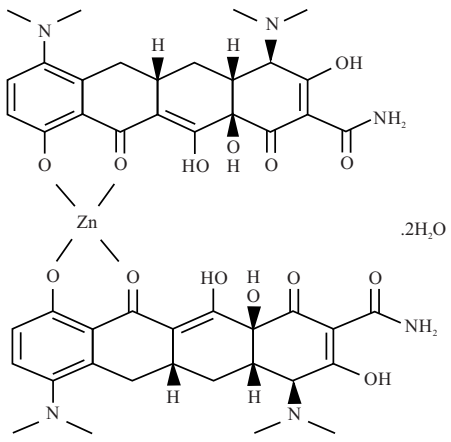

Fig. 3: Structure of Mino/Zn novel complex

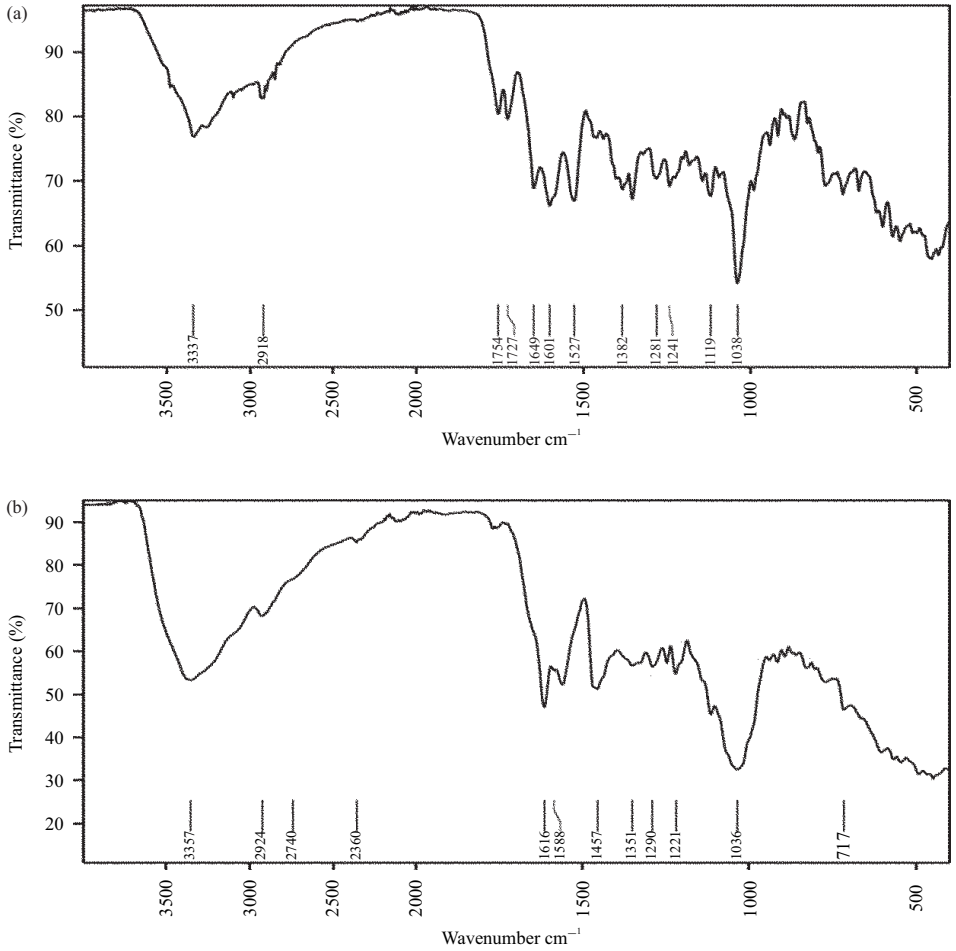

Fig. 4(a-b): FT-IR spectral analysis of (a) Minocycline and (b) Minocycline/Zn

Table 1: ^{1}H-NMR spectral assignments of minocycline and its zinc complex

Signals	Minocycline ligand	Mino/Zn(II)
^{1}H, CH	1.37, 2.80	2.85
^{1}H, H_2O	-	4.16, 4.38
^{1}H, OH alcoholic	4.86	4.89
^{1}H, aromatic ring	6.80, 7.38	6.85, 7.50
^{1}H, OH phenolic	9.42	9.98
^{1}H, NH amide	14.85	14.83

shows a loss in wt., up to 668°C, concluding that the loss in wt., for Zn(II) complex corresponds to the decomposition of minocycline ligand. The thermal decomposition steps for zinc complexity are three steps. From the thermogram of zinc complexity, ZnO was the most stable final product contaminated with some carbon atoms.

XRD, SEM and TEM investigations: To confirm the structure of the zinc/Mino complex, X-ray diffraction was carried out in Fig. 8. The XRD patterns elucidate the crystallinity arrangement for the complexity. At room temperature, Mino and its zinc complex were investigated by X-ray diffraction using Cu Kα radiation. The diffractograms were examined between 10-80°. The crystalline size is calculated using the Scherrer formula as discussed by El-Megharbel *et al.*[54]:

$$D = \frac{k\lambda}{\beta Cos\theta}$$

where, k is a constant and equal to 0.94, l the wavelength of X-ray used (0.154 nm) and b is full in width at half maxima peak of XRD pattern. The calculated crystalline size for zinc complexity was found to be 7 nm.

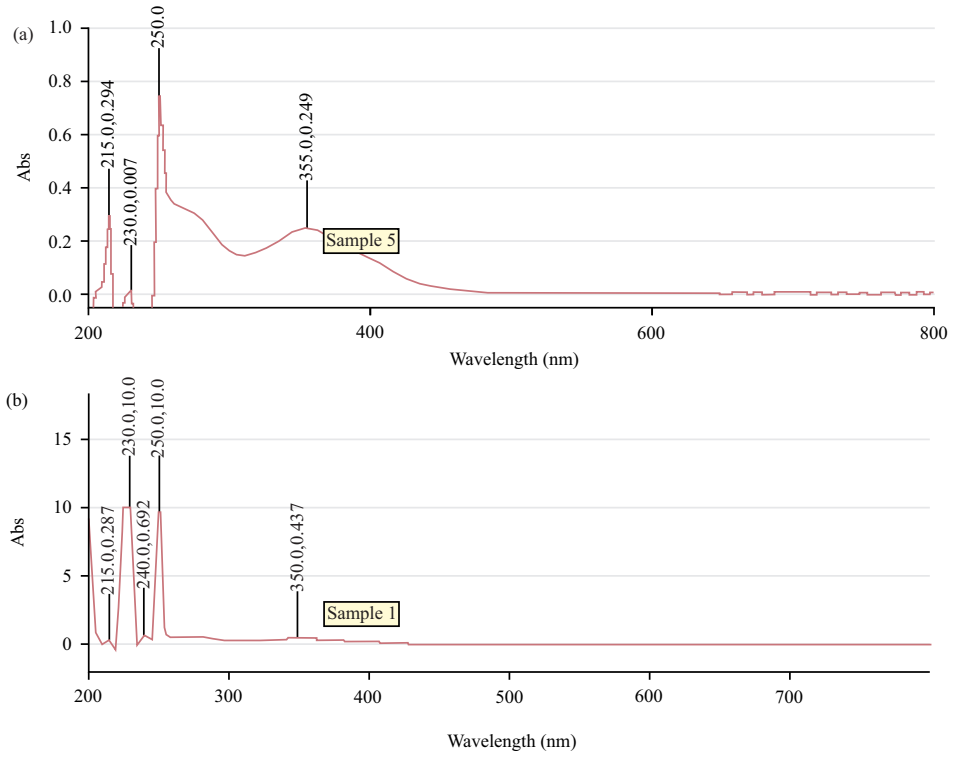

Fig. 5(a-b): UV-Vis spectral analysis of (a) Minocycline and (b) Minocycline/Zn

The TEM images for Mino and its Zn(II) complexity are described in Fig. 9(a-b). The orderly matrix for Mino and its zinc chelate in the pictograph was clarified. This confirms that the zinc Mino complex has a homogeneous phase material. A spherical black spots-like shape has appeared in zinc/Mino chelate with particle sizes ranging from 7-19 nm.

The SEM images for Mino and its zinc complex are in Fig. 9(c-d). The images show that the size of the particles is small and located within nano range. The surface morphology for minocycline and $[Zn(Mino)_2]\cdot 2H_2O$ showed that all particles had more ability to agglomerate formation due to homogeneity in size. The Mino and its zinc compound appeared as small rectangular projections.

Cytotoxicity activity (IC_{50} determination): The cellular inhibitory concentration (IC_{50}) of the cells' viability was detected by using MasterPlex 2010 software. The viable cells percentage at conc. 10 ug/mL of (Mino/Zn) was 59.30 µg/mL, meanwhile, at conc. 100 ug/mL of novel complex (Mino/Zn) was 7.98 µg/mL, which proved the novel potent record of the novel synthesized complex of Mino/Zn in inhibition of lung cancer cells growth to very low cellular viability percentages as appeared in via the faint color in column of cellular viability test on the well plate at conc.100 ug/mL which indicates the death of most lung cancer cells very clearly (Fig.10a).

Histogram of molecular docking simulations and heat map analyses: The SARS-CoV ligand-protein of the novel complex Mino/Zn complex within ACE2 and M^{Pro} histograms during the simulation time of 100 ns are shown in (Fig.10b). During the first docking phase, the formula (Mino/Zn) is redocked against the Angiotensin-Converting Enzyme-2 (ACE2), which may have a protective effect on COVID-19 patients by reducing the severity of respiratory symptoms. Moreover, the main protease for SARS-CoV-2, M^{pro} is redocked against the virus, which is its key enzyme and plays a crucial role in mediating transcription and viral replication (Fig. 11a-b), respectively. The conclusions can be drawn by examining the docking results of our newly synthesized complex against SARS-CoV's ACE2 pockets and M^{pro} and taking into account the previously discussed pharmacokinetic properties, we can conclude the following: The redocked cocrystallized formula formed hydrogen bonds with GLN-102, LEU-100, SER-106 and ASN-117 in case of ACE2 receptor and ASN-303, ALA-295, SER-333 and GLN-487 in case of M^{Pro} receptor, with a high level of activity.

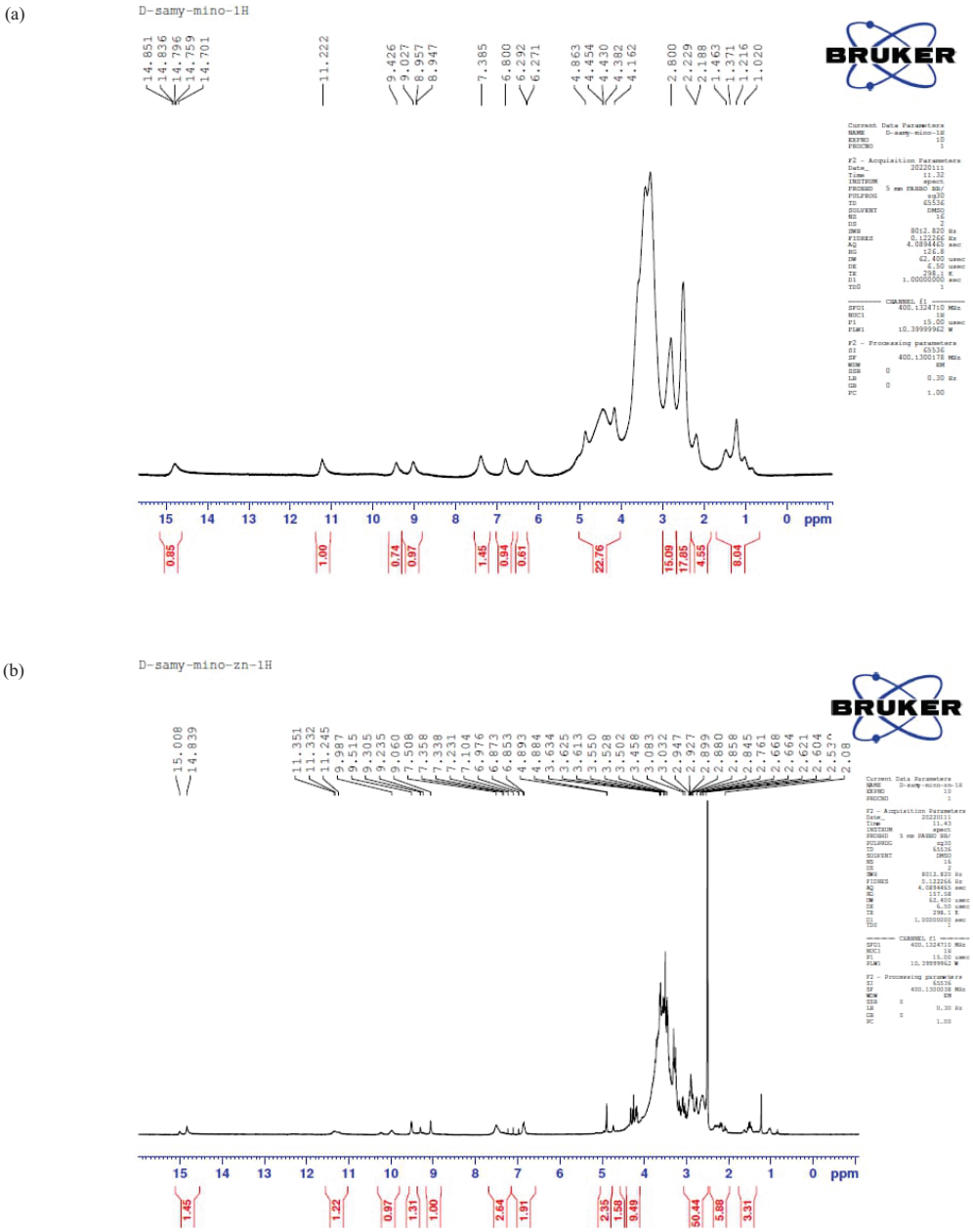

Fig. 6(a-b): ^{1}H-NMR for (a) Mino free ligand and (b) Mino/Zn novel complex

The most involved amino acid in the hydrogen bond interactions involving the Mino/Zn complex with ACE2 was LUT 100, which contributed roughly 97% and ALA 99, which contributed roughly 90% (Fig. 11 and 12a).

Furthermore, figure describes the SARS-CoV ligand-protein of Mino/Zn complex with M^{Pro} during (100 ns) simulation time. The ASN 303 and SER 333 each contributed roughly 42 and 83%, respectively, of the interactions as H-bonding in the Mino/Zn complex with M^{Pro} (Fig. 11 and 12b).

Ligand properties and RMSD analysis: Heat maps are displayed in Fig. 13(a-b) along with ligand features such as the RMSD, Radius of Gyration (rGyr), (SASA) which is solvent accessible surface area, Intramolecular Hydrogen Bond (intraHB), molecular surface area (MolSA) and polar surface area (PSA). The Root Mean Square Deviation (RMSD) provides information on additional ligand properties.

For the Mino/Zn complex with ACE2, the RMSD and rGyr were found to be between 0.6-4.8 and 1.8-4.8 Å. Additionally, during the 100 ns of simulation, intraHB with

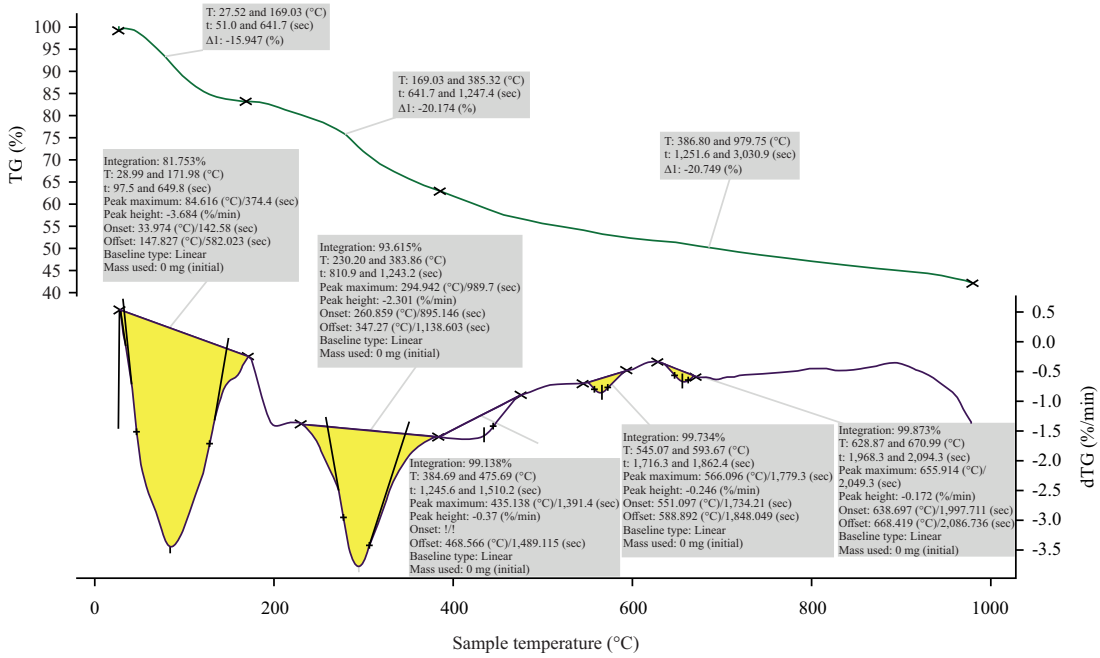

Fig. 7: TGA of Mino/Zn novel complex

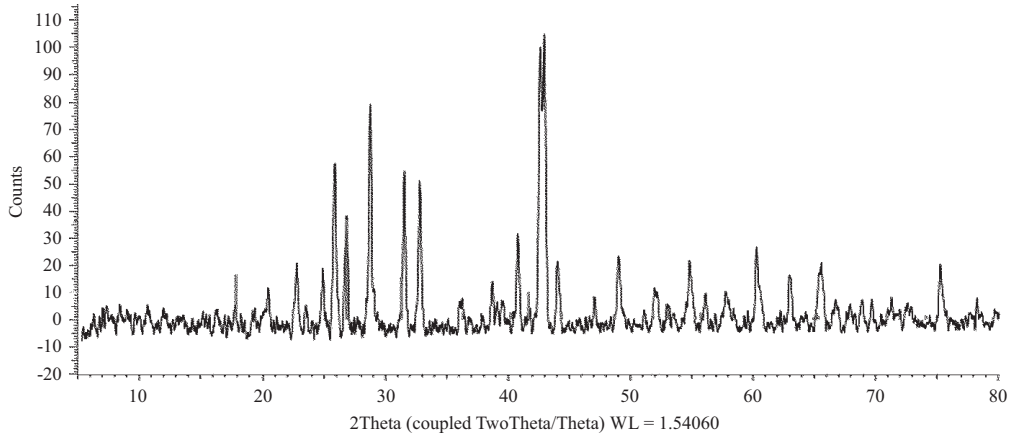

Fig. 8: XRD of Mino/Zn novel complex

many bands was observed to range from (1.1-4) and the MolSA range within (312–345.5 Å2). Furthermore, the SASA was ranged between (48-200 Å2). Additionally, its PSA ranged from 40 to 285 Å2 (Fig. 14a-b).

The RMSD and rGyr for Mino/Zn complex with M^{Pro}, all were observed to be within the range of (0.2-2.25) and (1.4-2.20), respectively. Also, intraHB with bands were ranged from (0-4) Å and the MolSA ranged between (80-90 Å2). Additionally, SASA range was within (100-600 Å2). Additionally, its PSA ranged within 56 and 280 Å2 (Fig. 14a-b).

During the simulations, the impact of the novel formula on the stability of ACE2 and M^{Pro} receptors was observed by analyzing the RMSD values of Cα atoms for the Mino/Zn complex. As shown in (Fig. 14a-b), the outcomes were plotted against the simulation's time. With RMSD values of less than 5.00 Å, the protein's fluctuation was within an acceptable range, suggesting that the protein conformation was stable before reaching equilibrium.

The ligand properties displayed significant torsion and fluctuation at the start of 100-ns simulation (Fig. 15a-b). This suggests that the Mino/Zn complex is highly stable at the SARS-CoV-2 main protease active site, as demonstrated by the clear in simulation (Fig. 16).

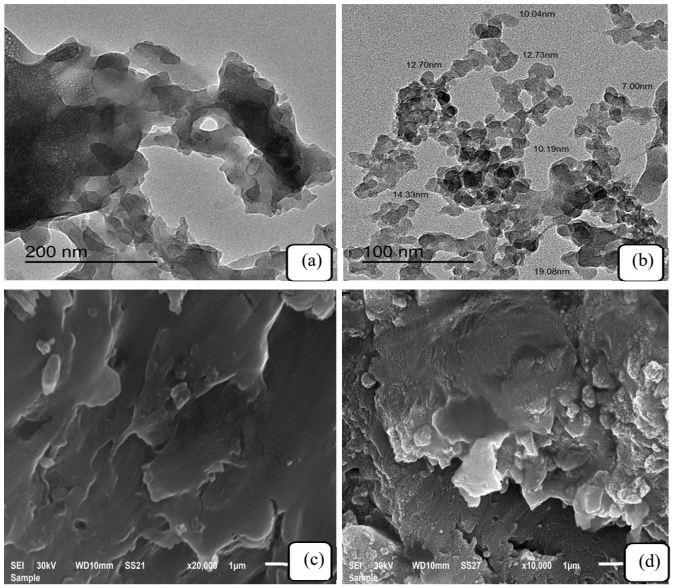

Fig. 9(a-d): TEM sections (a) Minocycline, (b) Minocycline/Zn, SEM sections, (c) Minocycline and (d) Minocycline/Zn
(a) Orderly matrix for Mino was clarified with a homogeneous phase material, (b) A spherical black spots-like shape has appeared in Mino/Zn chelate with particle sizes ranging from 7-19 nm, (c) Minocycline with plan surface within small molecules and (d) Surface morphology for minocycline/Zn showed that all particles had agglomerated due to homogeneity in size and appeared as small rectangular projections

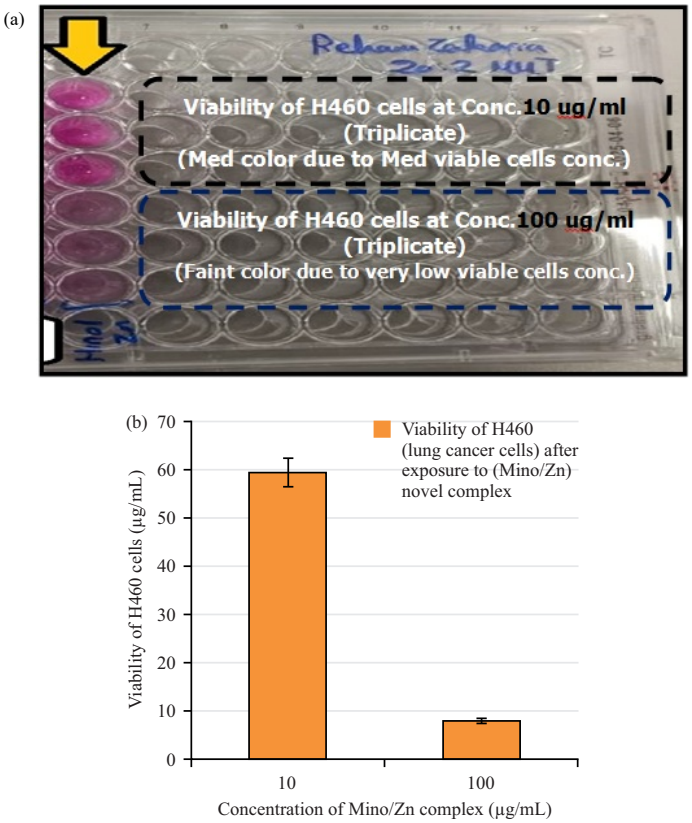

Fig. 10(a-b): Cytotoxicity assay of Mino/Zn on lung cancer cells (H460), (a) Cellular viability test on the well plate at conc.100 µg/mL which indicates the death of most lung cancer cells very clearly and (b) SARS-CoV ligand-protein of the novel complex Mino/Zn complex within ACE2 and M^{Pro} histograms

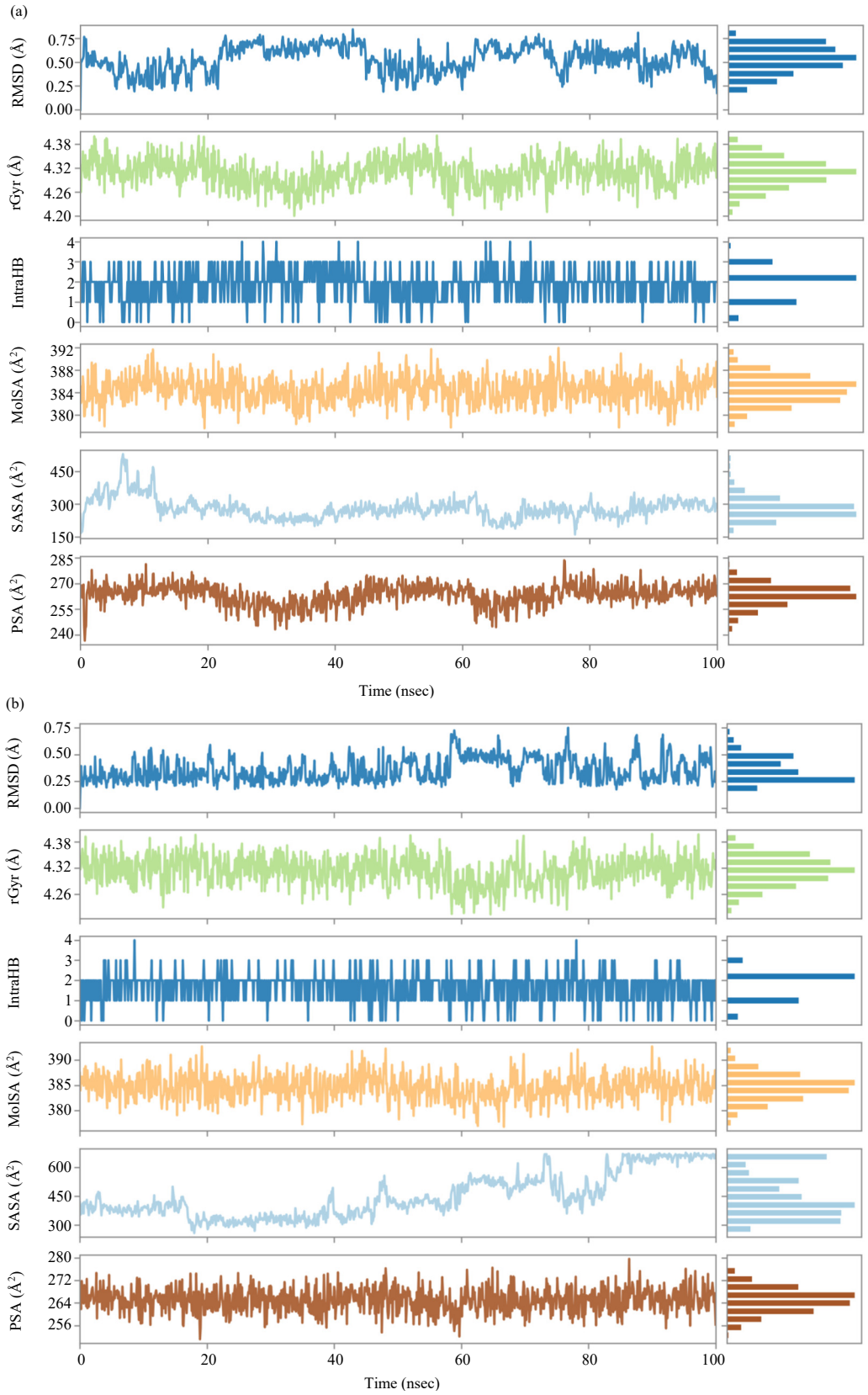

Fig. 11(a-b): Histogram shows the interactions between the tested ligand (Mino/Zn) and the SARS-CoV-2 receptors over a 100-ns simulation period for two different receptor types: (a) ACE2 and (b) M^{Pro}

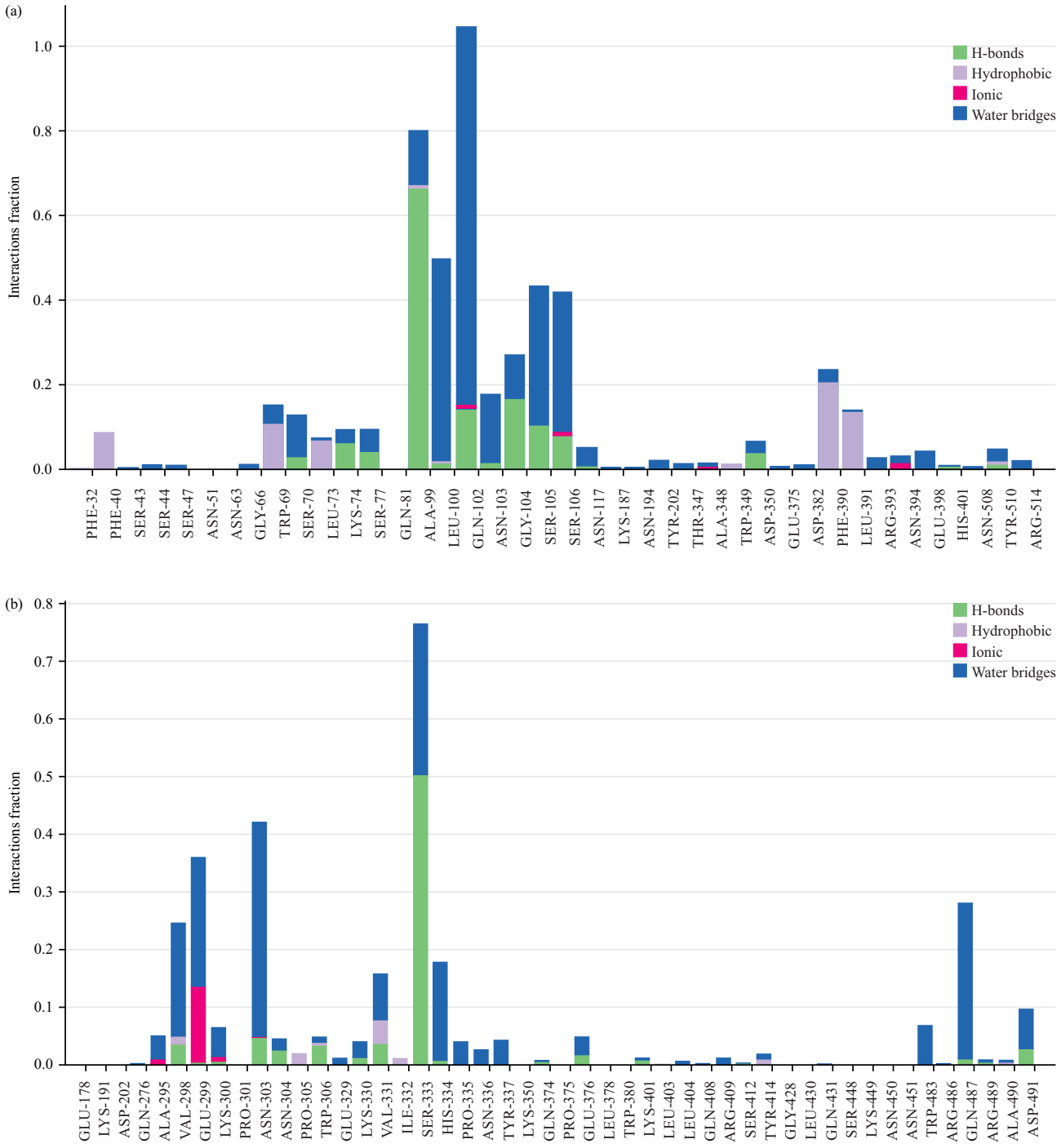

Fig. 12(a-b): Properties of the novel Mino/Zn complex's ligand for Mino/Zn interactions with the receptors of SARS-CoV-2 over the course of 100 ns simulation's for (a) ACE2 and (b) M^{Pro} receptors

Histological and immunohistological sections: The immunohistological sections showing sections in lung tissues of control group with normal alveoli and inter-alveolar septa (Fig. 17a), ACR treated group (Fig. 17b), Mino/Zn treated group (Fig. 17c) and ACR plus Mino/Zn treated group (Fig. 17d) (H&E ×200).

Immunostaining sections in the lung tissues of control group showing negative caspase-3 immunostaining (Fig. 18a),

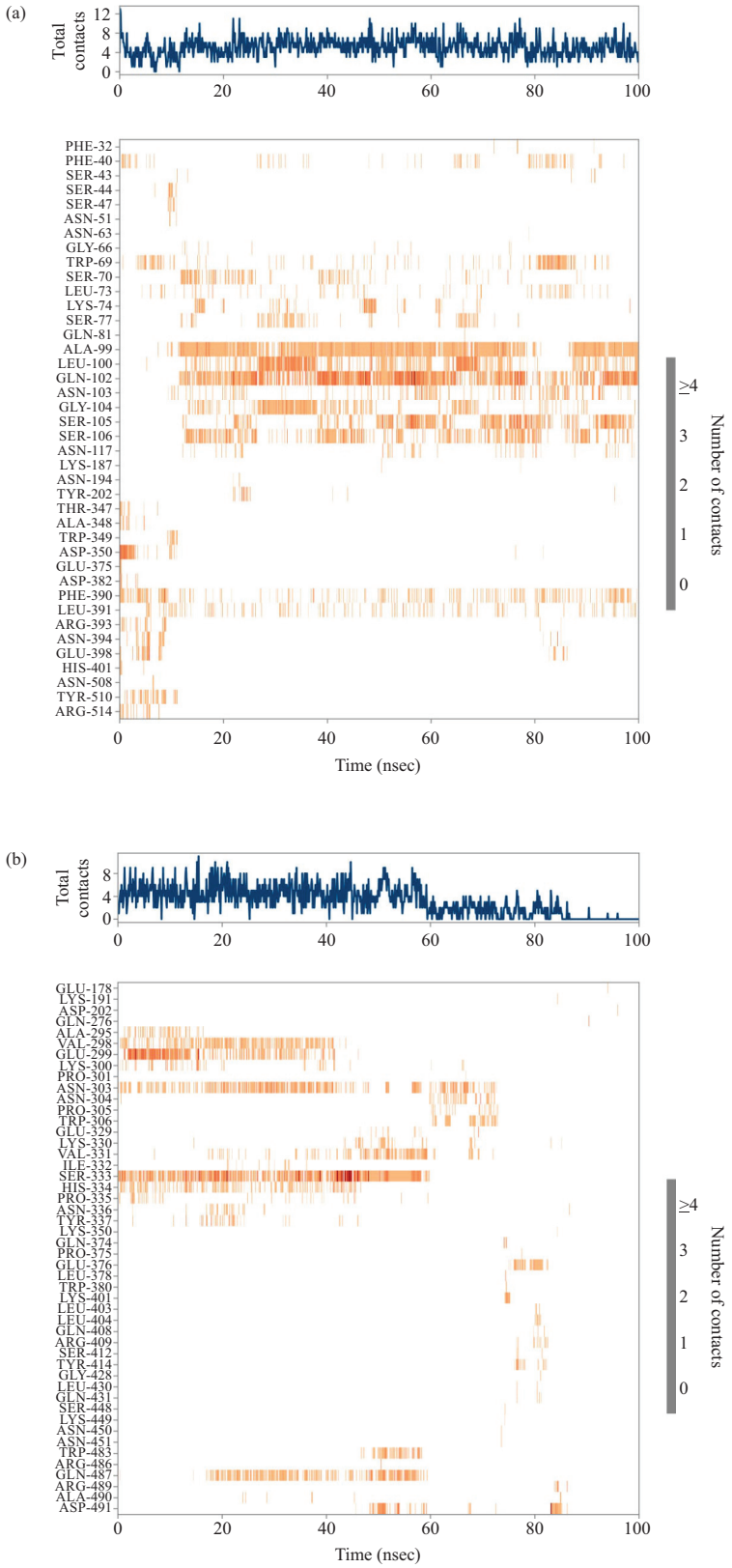

Fig. 13(a-b): Heat map of Mino/Zn novel complex for SARS-CoV protein-ligand receptors all over the 100 nsec of simulation for (a) ACE and (b) M^{Pro}

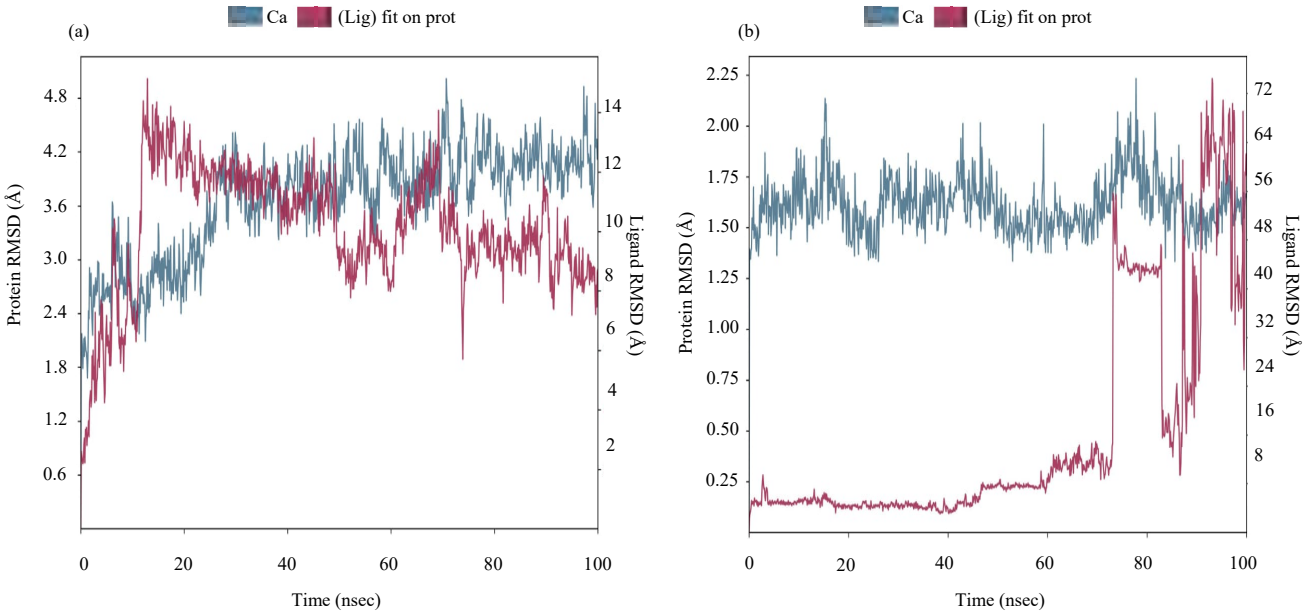

Fig. 14(a-b): RMSD of the Cα atoms in Mino/Zn novel complex for the SARS-CoV receptor, (a) ACE2 and (b) M^{Pro} against time

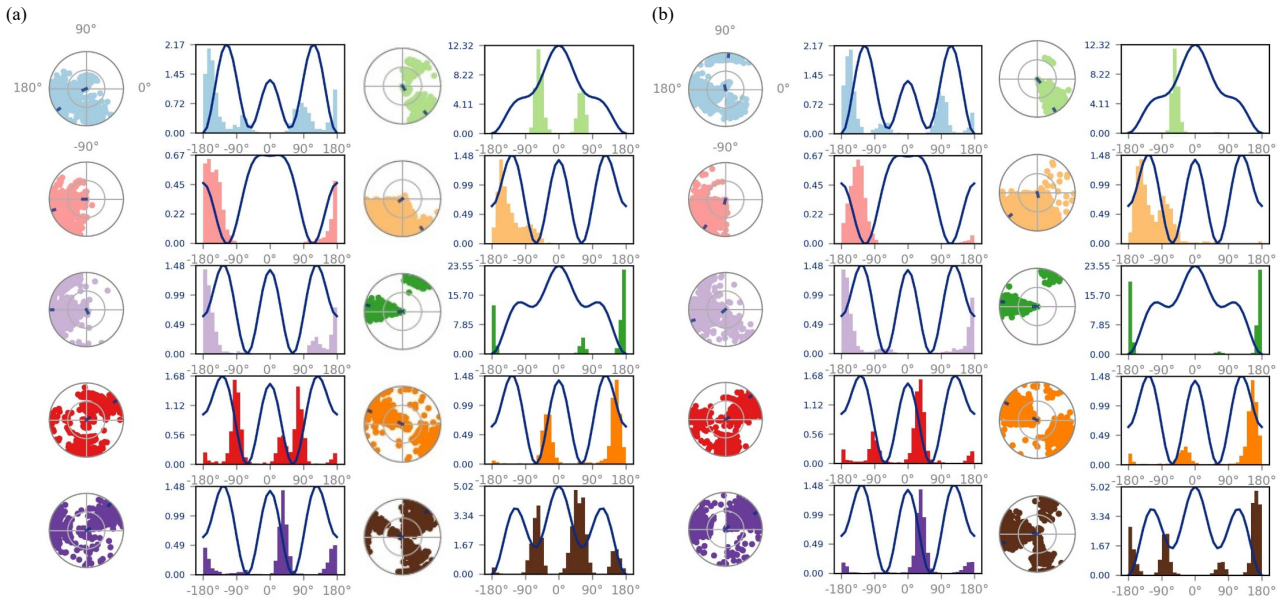

Fig. 15(a-b): Ligand torsion profile of Mino/Zn novel complex with (a) ACE2 and (b) M^{Pro} of simulation (100 ns)

ACR group showing marked and significant caspase-3 immunoreactivity (Fig. 18b), Mino/Zn treated group revealed very mild immunostaining (Fig. 18c) and ACR plus Mino/Zn treated group showing mild immunostaining to caspase-3 (Fig. 18d).

Antibacterial activity evaluation: Bacteria classified as Gram-positive (*Bacillus subtilis*; ATCC 6633), Gram-negative (*Staphylococcus aureus*; ATCC 6538) and (*Escherichia coli*; ATCC 8739) were used to evaluate the target complexes biologically. Figure 12 presents the findings of the antimicrobial activities of the Mino/Zn metal complex. The Mino/Zn complex was found to be sufficient, with high antimicrobial activities against various bacterial strains. The inhibition concentrations of the complex against both Gram-positive and Gram-negative bacteria (*B. subtilis*,

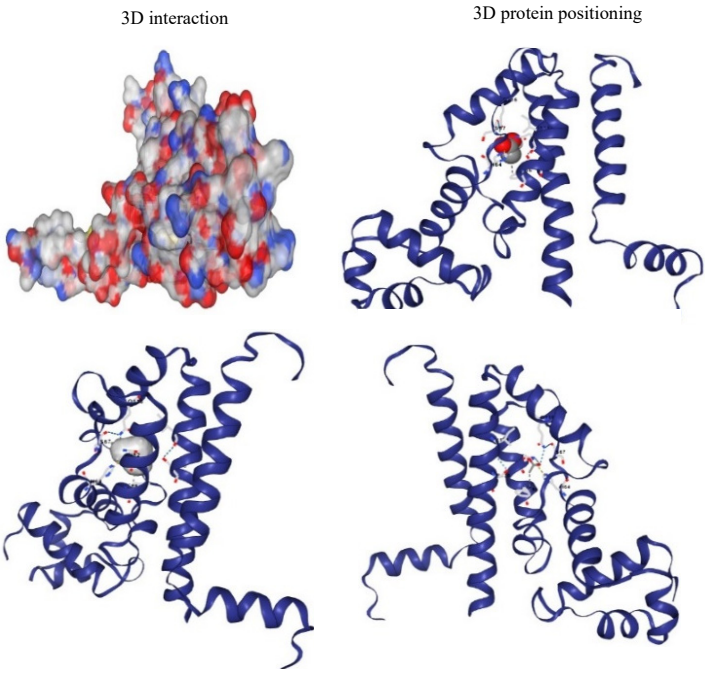

Fig. 16: 3D view of binding interactions and the 3D positioning between the tested Mino/Zn and ACE2 binding pocket receptor of SARS-CoV-2

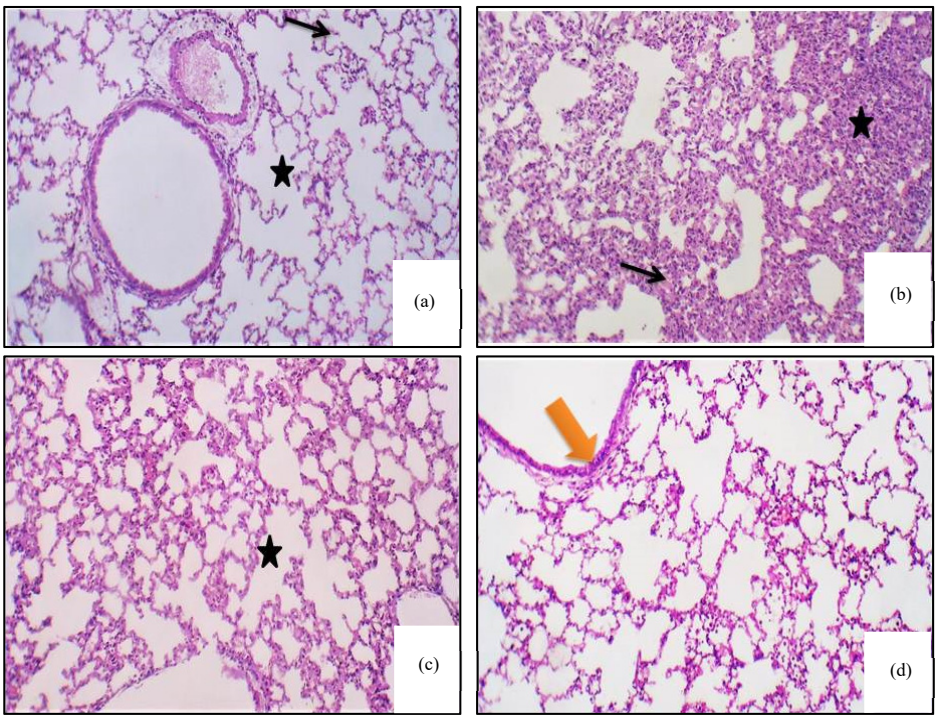

Fig. 17(a-d): Section in lung tissues of (a) Control group, (b) ACR treated group, (c) Mino/Zn treated group and (d) ACR plus Mino/Zn treated group

(a) Normal alveoli (Black star) and inter-alveolar septa (Thin arrow), (b) Loss of normal pulmonary architecture with pulmonary thickening (Black star) of alveolar wall and the marked interstitial inflammatory infiltrates (Black arrow), (c) Partial subside of inflammation with mild thickening of some alveoli (Black asterisk) and (d) Showing normal architecture of lung subside of the mild thickening of alveolar wall and the inflammatory infiltrate (Orange arrow) (H&E x200)

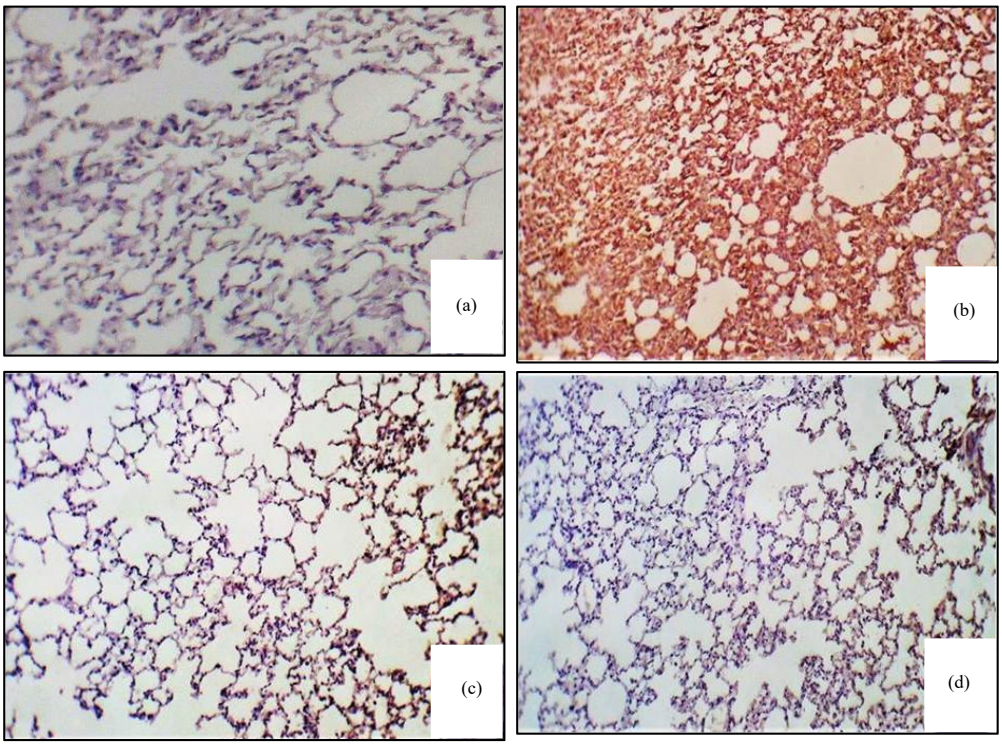

Fig. 18 (a-d): Immunostaining sections in the lung tissues of (a) Control group, (b) ACR group, (c) Mino/Zn treated group (320 µm) and (d) ACR plus Mino/Zn treated group (DAB chromogen, Meyer's hematoxylin counterstain)

(a) Negative caspase-3 immunostaining (negative immunoreactivity), (b) Marked and significant caspase-3 immunoreactivity (heavy immunoreactivity), (c) Revealed very mild immunostaining (very mild immunoreactivity) and (d) Mild immunostaining to caspase-3 (mild immunoreactivity) scale bar: 320 µm

S. aureus and *E. coli*) were found to be high at extremely low concentrations for *E. coli*, 0.625 mg/mL and 0.009 for *B. subtilis*, 0.625 for the Mino/Zn against *S. aureus* (Fig. 19).

DISCUSSION

The world has an urgent need to evolve new antibacterial generations with high efficacy and minimal side effects in order to alleviate antibiotic resistance, a byproduct of antibiotic misuse. This need has arisen due to a highly evolved percentage of antibacterial resistance. Therefore, the novel antibiotic metal drug complexes might develop new properties as strong antioxidant, anticancer and anti-inflammatory agents. This is a new scientific trend for improving the activities of antibiotics and reducing their adverse effects on multiple organs.

Tetracyclines are bacteriostatic antibiotics that are effective against a variety of Gram +ve and -ve bacteria, both anaerobic and aerobic. Their fundamental chemical structure is a tetracyclic naphthacene carboxamide ring with substituents at various positions; However, structural changes, such as those that alter ring D through carbon locations C7-C9, have been developed in an attempt to increase the effectiveness of this class of antibiotics. The increased efficacy seen with semisynthetic compounds like minocycline was caused by these modifications. The FDA currently approves the use of minocycline (Mino) (7-dimethylamino-6-dimethyl -6-deoxytetracycline), a semi-synthetic, second-generation tetracycline analogue, for the treatment of rheumatoid arthritis, acne vulgaris and some STDs[55]. When Mino is taken orally, it exhibits a better pharmacokinetic profile than its parent drug which is tetracycline: It is quickly and fully absorbed, has a longer half-life with nearly high bioavailability[56] and, perhaps most remarkably, has a solid safety record when taken over an extended period of time. Furthermore, it is a very lipophilic molecule that easily crosses the blood-brain barrier[57], which makes it useful for treating a variety of diseases affecting the central nervous system[58]. Numerous studies conducted recently have focused on the non-antibiotic properties of minocycline, such as its ability to inhibit proteolysis, suppress angiogenesis and tumor metastasis and have anti-inflammatory and anti-apoptotic

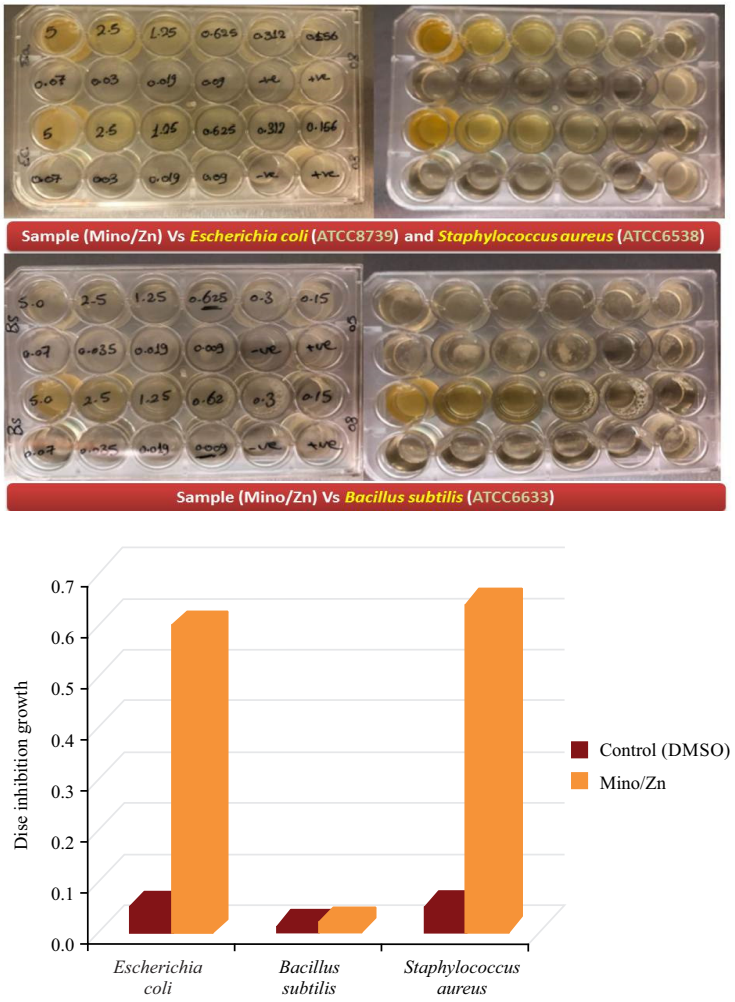

Fig. 19: Bacterial disc inhibition growth for the tested bacterial strains

properties[59]. These studies support minocycline's use in the treatment of autoimmune disorders, including rheumatoid arthritis, inflammatory bowel diseases and cancer.

The current study's results were greatly supported by the earlier research, which also demonstrated the great potential of the novel Mino/Zn complex. Specifically, the complexation between Zn and Mino antibiotics enhanced Mino's bioavailability and afforded novel capacities involving declining the inflammatory series, enhancing pulmonary functions and elevating the efficacy of pulmonary tissue structure. One particularly promising result was the high percentage of lung cancer cells that were inhibited from proliferating. This is a novel finding that deserves significant attention and additional clinical studies to confirm its accuracy and improve its complexation structure to be used clinically to decline the widespread antibiotic resistance.

Regarding the chemical spectroscopic characterization of the novel complex Mino/Zn, the current data demonstrated the great ability of the novel complex of Mino/Zn to penetrate the pulmonary tissues and improve its functions and alleviate the inflammation markers either biochemically or structurally, as well as via the declining of the caspase-3 marker's expression. This was in accordance with the previous findings that confirmed that, when used orally, Mino as an antibacterial drug shows a better pharmacokinetic profile than its parent, tetracycline: It is rapidly and completely absorbed and importantly shows excellent tissue penetration[59].

Interestingly, Mino has also been identified as the most effective tetracycline derivative in terms of neuroprotection, this effect has been verified in a number of experimental models of brain injury, as well as in a number of neurodegenerative conditions[60] and the novel pulmonary

protective effect demonstrated by biochemical and structural analysis in the current study against oxidative stress and the toxic effects of acrylamide.

The precise mode of action underlying Mino antibiotics' anti-inflammatory and immunomodulatory effects is not fully understood, despite the fact that their antibiotic qualities are well understood. However, the novel ameliorative effects of the current novel complex Mino/Zn, prove its prospective mechanism of action as proved in previous studies such as (a) Inhibitory effects on enzyme activities[61]; (b) Antioxidant properties[62] and (c) Inhibition of caspase-3 activation[63]; It's interesting to note that some of these biological activities may be explained by the chelation of Mino with zinc metal, which is made possible by tetracyclines' well-known ability to bind Ca^{2+} and Mg^{2+} previously.

Minocycline displays antioxidant properties, but in the current study the novel complex of Mino/Zn showed high potent antioxidant activity against the increased production of reactive oxygen species under pulmonary pathological conditions and the severe inflammation that leads to the severe oxidative destruction or dysfunction of many cellular constituents as confirmed by Park and Lucchesi[64], as the same context, as tetracyclines are particularly versatile in their ability to combat oxidative stress and scavenge free radicals[65] and this confirmed the novelty of the current results that showed novel antioxidant capacities of Mino as a member of modified tetracycline after chelation with Zn metal.

These antioxidant properties of the novel synthesized Mino/Zn are consistent with the chemical nature of Mino, as its chemical structure with presence of substituted phenol ring, which is similar to the nature of vitamin E and thus belongs to the class of phenolic antioxidants. Indeed, Mino has proven to have direct antioxidant effects in a number of cell-free mixed-radical assays[66,67], with its ability to scavenge radicals being on par with vitamin E and not requiring Fe^{2+} chelation. In particular, because Mino interacts directly with these free radicals[68], it has been demonstrated to be highly effective in quenching H_2O_2[69] and scavenging superoxide ions[70,71]. The current results proved that Mino/Zn novel complex was highly potent with a potent half maximal Inhibitory Concentration (IC_{50}) value in inhibition of large lung cancer cells (H460) more potent and higher that the anti-carcinogenic activity of Mino alone, as the current results proved that Mino/Zn inhibited the growth of H460 cells by 59.30% percentage at concentration 10 ug/mL. Meanwhile Mino/Zn inhibited the proliferation of H460 by 7.98% at concentration 100 ug/mL.

Zinc plays a vital biological role in enhancing antioxidant defense mechanism and elimination of viral infection, as proved by El-Megharbel *et al.*[42] and Al-Salmi *et al.*[72]. The Zn is vital for potent cellular protection and for eradicating viruses from the cellular hosts. The Zn influences several regulators, including antibacterial and can be used for inhibition of cancer cells[42,72]. The spectroscopic characterization of the current complex is in great accordance with the novel characteristic of potent active compounds and flavonoids previously proved El-Megharbel *et al.*[42] and Hamza *et al.*[73], the chelation between Mino and Zn metal greatly enhances its bacterial activities which record novel data on bacterial inhibition of Mino/Zn complex against *E. coli* in concentration 0.625 mg/mL and high inhibition of *B. subtilis* at 0.009 mg/mL and inhibition of *S. aureus* at 0.625 mg/mL.

The Mino has shown direct antioxidant effects in multiple cell-free mixed-radical assays[66], with its radical scavenging activity being independent of Fe^{2+} chelation and on par with vitamin E. In particular, because Mino interacts directly with these free radicals[67], it has been demonstrated to be highly effective in scavenging of H_2O_2[67,68], scavenging superoxide[68]. The Mino was 200-300 times more potent than tetracycline and in agreement with the current findings, Mino with Zn complex afforded significant antioxidant capacities against free radicals and oxidative injury induced by ACR and amelioration of pulmonary tissues either structurally or immunologically.

Furthermore, it was discovered that mino had 200 times the potency of tetracycline in terms of inhibiting lipid peroxidation[66,67]. It is believed that the diethylamino group on the phenolic carbon of the Mino/Zn novel complex, which is exclusive to Mino among tetracyclines and offers enhanced steric hindrance, is the primary cause of its superior scavenging ability[68]. In addition to the strong antiviral, antibacterial and immunological properties of zinc, which have been amply demonstrated in a previous study of El-Megharbel *et al.*[23], these results also strongly supported the strong antioxidant properties of the Mino/Zn unique complex, which have been demonstrated to reduce lipid peroxides, reduce free radical damage and improve lung tissue structure.

By attenuating innate and adaptive immunity and blocking apoptotic cascades, mino has been shown to mitigate cellular death[68]. This has a broad anti-inflammatory effect and protects cells in a range of experimental models. It has been demonstrated that it interferes with a variety of apoptotic processes, including caspase inhibition. Given that the effects of Mino cytoprotective activity were eliminated when Bcl-2 was down-regulated in the cells, these effects appear to be crucial[74]. Minocycline concurrently suppresses the expression of pro-apoptotic proteins like Fas[75,76] and Bax[75]. Additionally, it lessens p53 up-regulation, which stops the

mitochondria's outer membrane permeabilization pore from forming, preventing cyt c. This stops the release of cyt c and SMACs proteins, which ultimately blocks the downstream caspase activation that triggers apoptosis[77,78].

For many years, Gram -ve and Gram +ve bacteria infections have been treated with mino. The Mino is typically prescribed to treat a number of illnesses, such as urinary tract infections and acne[78]. On the other hand, a lot of research and discussion has recently focused on Mino's varied non-antibiotic effects. Prior experimental research revealed that Mino can be used as a neuroprotective agent against Alzheimer's disease. This finding confirmed our concept by the great capacities of the Mino novel complex with Zn in alleviation of oxidative stress and prevention of apoptosis and also eventually alleviating the carcinogenic activities of cancer cells, as the unique result for this study proved the highly potent anti-carcinogenic activity of Mino/Zn in inhibition of large lung cancer cells (H460) which is a novel result with great concept and great inhibition of cancer cell's growth.

The current study mimics the potential for acute respiratory distress syndrome and multiple organ failure in COVID-19 patients by inducing pulmonary toxicity through the use of ACR. Inflammatory cytokine storm has been observed in these patients. The Mino has been reported previously to exert anti-inflammatory, immunomodulatory and even antiviral effects in addition to its broad antibacterial activity. The possibility of antiviral activity against SARS-CoV-2 has also been suggested by several researchers of Hamza *et al.*[79]. All these findings support the current finding of great activity of Mino/Zn novel complex and it's possible affinity for binding for the main protease enzyme receptor (M^{Pro}) and main SARS-CoV-2 receptor (ACE2) with all chemical characterization and spectroscopic studies which confirmed via XRD the crystalline form of the prepared novel complex Mino/Zn and it's new bands which confirm the presence of potent chelation between Zn^{2+} and donation sites in Mino and it's prospective activity against SARS-CoV-2 via the molecular docking studies.

Clinical recommendations typically state against using antibiotics to treat viral infections due to improper and excessive use of these drugs. However, because of their antiviral and anti-inflammatory properties, a number of antibiotics have been suggested as repurposing medications during the COVID-19 pandemic. Multiple therapeutic targets have been identified for SARS-CoV-2, with the main protease (M^{Pro}) implicated in the transcription and replication of the viral genome[79]. The novel Mino/Zn complex has demonstrated great potency against SARS-CoV-2, as demonstrated by ligand properties, ligand torsion, RMSD and heat maps. These findings greatly confirm the potency of Mino/Zn against SARS-CoV-2.

According to Shamkani *et al.*[10], a pneumonia model was created by intraperitoneally giving *A. baumannii* suspension to anesthetized mice whose immune systems had been twice compromised by cyclophosphamide, confirming the current finding and mitigating the effects of the novel Mino/Zn complex. The mice given the combination of two compounds required less time to treat than the animals given the single medication Mino. The lung infection of the mouse with *A. baumannii* was confirmed and the niosomes contained both GaN and Mino. The Mino and GaN-loaded niosomes could be considered promising candidates to treat the infections caused by *A. baumannii* biofilm, a similar mimic idea but with chelation of Mino with Zn metal ion that greatly enhanced the pulmonary functions and alleviated the pulmonary toxicity by restoring the normal pulmonary structure.

CONCLUSION

Minocycline/Zinc (Mino/Zn) novel complex was synthesized and characterized using elemental analysis, spectroscopic methods IR, ^{1}H-NMR, UV, X-ray diffraction, magnetic susceptibility, SEM and TEM. For Zn/Mino novel complex, TEM revealed the formation of spherical black spots with a particle size range of 7-19 nm. Thus, using simulation molecular docking, it is possible to conclude that the novel Mino/Zn complex formula is a potent antioxidant, anticancer and antibacterial agent with the cellular anticipated inhibitory effect against SARS-CoV-2.

SIGNIFICANCE STATEMENT

The current study deals with novel potent and promising anticancer, antibacterial and antioxidant activities of Mino/Zn novel complex. This study is a novel important scientific trend in alleviation of the side effects of the antibiotics and synthesis of novel complexes with new potent capacities. Those novel complexes may help in elevation of the immune system during any pandemic and for saving community health.

ACKNOWLEDGMENT

The authors extend their appreciation to Taif University, Saudi Arabia, for supporting this work through project number (TU-DSPP-2024-155).

REFERENCES

1. Yang, G., Y. Cao, P. Wang, L. Mei, J. Chen and W. Lu, 2022. Minocycline pretreatment prevents blood-brain barrier disruption in septic rats. J. Surg. Res., 273: 247-254.
2. Yang, Y., V.M. Salayandia, J.F. Thompson, L.Y. Yang, E.Y. Estrada and Y. Yang, 2015. Attenuation of acute stroke injury in rat brain by minocycline promotes blood-brain barrier remodeling and alternative microglia/macrophage activation during recovery. J. Neuroinflammation, Vol. 12. 10.1186/s12974-015-0245-4.
3. Michels, M., A.S. Vieira, F. Vuolo, H.G. Zapelini and B. Mendonça *et al*., 2015. The role of microglia activation in the development of sepsis-induced long-term cognitive impairment. Brain Behav. Immun., 43: 54-59.
4. Higashida, T., C.W. Kreipke, J.A. Rafols, C. Peng and S. Schafer *et al*., 2011. The role of hypoxia-inducible factor-1α, aquaporin-4, and matrix metalloproteinase-9 in blood-brain barrier disruption and brain edema after traumatic brain injury. J. Neurosurg., 114: 92-101.
5. Pioletti, M., F. Schlünzen, J. Harms, R. Zarivach and M. Glühmann *et al*., 2001. Crystal structures of complexes of the small ribosomal subunit with tetracycline, edeine and IF3. EMBO J., 20: 1829-1839.
6. Al-Thubaiti, E.H., S.M. El-Megharbel, B. Albogami and R.Z. Hamza, 2022. Synthesis, spectroscopic, chemical characterizations, anticancer capacities against HepG-2, antibacterial and antioxidant activities of cefotaxime metal complexes with Ca(II), Cr(III), Zn(II), Cu(II) and Se(IV). Antibiotics, Vol. 11. 10.3390/antibiotics11070967.
7. Yang, Y.S., T.W. Huang, Y.C. Huang, W.C. Huang and S.Y. Hsu *et al*., 2022. *In vitro* and *in vivo* efficacy of minocycline-based therapy for *Elizabethkingia anophelis* and the impact of reduced minocycline susceptibility. Int. J. Antimicrob. Agents, Vol. 60. 10.1016/j.ijantimicag.2022.106678.
8. Hand, E., H. Davis, T. Kim and B. Duhon, 2016. Monotherapy with minocycline or trimethoprim/sulfamethoxazole for treatment of *Stenotrophomonas maltophilia* infections. J. Antimicrob. Chemother., 71: 1071-1075.
9. Ritchie, D.J. and A. Garavaglia-Wilson, 2014. A review of intravenous minocycline for treatment of multidrug-resistant *Acinetobacter* infections. Clin. Infect. Dis., 59: S374-S380.
10. Shamkani, F., S.M. Barzi, F. Badmasti, M. Chiani, E. Mirabzadeh, M. Zafari and M. Shafiei, 2023. Enhanced anti-biofilm activity of the minocycline-and-gallium-nitrate using niosome wrapping against *Acinetobacter baumannii* in C57/BL6 mouse pneumonia model. Int. Immunopharmacol., Vol. 115. 10.1016/j.intimp.2022.109551.
11. Ghalibaf, M.H.E., A. Rajabian, M. Parviz, M. Akbarian, S. Amirahmadi, F. Vafaee and M. Hosseini, 2023. Minocycline alleviated scopolamine-induced amnesia by regulating antioxidant and cholinergic function. Heliyon, Vol. 9. 10.1016/j.heliyon.2023.e13452.
12. Romero-Miguel, D., N. Lamanna-Rama, M. Casquero-Veiga, V. Gómez-Rangel, M. Desco and M.L. Soto-Montenegro, 2021. Minocycline in neurodegenerative and psychiatric diseases: An update. Eur. J. Neurol., 28: 1056-1081.
13. Li, L., X. Xing, Q. Li, Q. Zhang, L. Fu and Y. Liu, 2021. Minocycline improves learning and memory functions in ischemic stroke rats via reduction of cerebral ischemia-induced neuroinflammation and apoptosis. Trop. J. Pharm. Res., 20: 287-292.
14. Zhang, J., M. Boska, Y. Zheng, J. Liu, H.S. Fox and H. Xiong, 2021. Minocycline attenuation of rat corpus callosum abnormality mediated by low-dose lipopolysaccharide-induced microglia activation. J. Neuroinflammation, Vol. 18. 10.1186/s12974-021-02142-x.
15. Parvardeh, S., M.A. Sheikholeslami, S. Ghafghazi, R. Pouriran and S.E. Mortazavi, 2022. Minocycline improves memory by enhancing hippocampal synaptic plasticity and restoring antioxidant enzyme activity in a rat model of cerebral ischemia-reperfusion. Basic Clin. Neurosci., 13: 225-236.
16. Sharma, V.K., A. Goyal and S.G. Sarm, 2010. Minocycline decreases acetylcholinestrase activity in intra-cerebroventricular streptozotocin infused rats. Int. J. Pharm. Sci. Res., 1: 52-57.
17. Mehta, B.K. and S. Banerjee, 2019. Minocycline reverses diabetes-associated cognitive impairment in rats. Pharmacol. Rep., 71: 713-720.
18. Amirahmadi, S., F.D. Farimani, M. Akbarian, F. Mirzavi, M.H.E. Ghalibaf, A. Rajabian and M. Hosseini, 2022. Minocycline attenuates cholinergic dysfunction and neuro-inflammation-mediated cognitive impairment in scopolamine-induced Alzheimer's rat model. Inflammopharmacology, 30: 2385-2397.
19. Amirahmadi, S., M. Hosseini, S. Ahmadabady, M. Akbarian, K. Abrari, F. Vafaee and A. Rajabian, 2021. Folic acid attenuated learning and memory impairment via inhibition of oxidative damage and acetylcholinesterase activity in hypothyroid rats. Metab. Brain Dis., 36: 2393-2403.
20. Veleba, M. and T. Schneiders, 2012. Tigecycline resistance can occur independently of the *ramA* gene in *Klebsiella pneumoniae*. Antimicrob. Agents Chemother., 56: 4466-4467.
21. Hou, Y., G. Xie, X. Liu, G. Li, C. Jia, J. Xu and B. Wang, 2016. Minocycline protects against lipopolysaccharide-induced cognitive impairment in mice. Psychopharmacology, 233: 905-916.

22. Moini-Zanjani, T., S.N. Ostad, F. Labibi, H. Ameli, N. Mosaffa and M. Sabetkasaei, 2016. Minocycline effects on IL-6 concentration in macrophage and microglial cells in a rat model of neuropathic pain. Iran. Biomed. J., 20: 273-279.
23. El-Megharbel, S.M., M. Alsawat, F.A. Al-Salmi and R.Z. Hamza, 2021. Utilizing of (zinc oxide nano-spray) for disinfection against "SARS-CoV-2" and testing its biological effectiveness on some biochemical parameters during (COVID-19 pandemic)-"ZnO nanoparticles have antiviral activity against (SARS-CoV-2)". Coatings, Vol. 11. 10.3390/coatings11040388.
24. Gervasi, F. and F. Pojero, 2024. Use of oleuropein and hydroxytyrosol for cancer prevention and treatment: Considerations about how bioavailability and metabolism impact their adoption in clinical routine. Biomedicines, Vol. 12. 10.3390/biomedicines12030502.
25. Shahzadi, C., A.D. Serafino, E. Aruffo, A. Mascitelli and P.D. Carlo, 2023. A549 as an *in vitro* model to evaluate the impact of microplastics in the air. Biology, Vol. 12. 10.3390/biology12091243.
26. Giard, D.J., S.A. Aaronson, G.J. Todaro, P. Arnstein, J.H. Kersey, H. Dosik and W.P. Parks, 1973. *In vitro* cultivation of human tumors: Establishment of cell lines derived from a series of solid tumors. JNCI: J. Natl. Cancer Inst., 51: 1417-1423.
27. Hamza, R.Z., E.H. Al-Thubaiti and A.S. Omar, 2019. The antioxidant activity of quercetin and its effect on acrylamide hepatotoxicity in liver of rats. Lat. Am. J. Pharm., 38: 2057-2062.
28. Xia, X., Z. Zhang, C. Zheng, Q. Deng, M. Zheng, L. Han and X. Xiang, 2020. Ameliorative effects of canolol against acrylamide toxicity in PC12 cells through modulating MAPKs pathway and autophagy. J. Funct. Foods, Vol. 75. 10.1016/j.jff.2020.104257.
29. Houdkova, M., A. Chaure, I. Doskocil, J. Havlik and L. Kokoska, 2021. New broth macrodilution volatilization method for antibacterial susceptibility testing of volatile agents and evaluation of their toxicity using modified MTT assay *in vitro*. Molecules, Vol. 26. 10.3390/molecules26144179.
30. Liu, D. and K. Kwasniewska, 1981. An improved agar plate method for rapid assessment of chemical inhibition to microbial populations. Bull. Environ. Contam. Toxicol., 27: 289-294.
31. Skehan, P., R. Storeng, D. Scudiero, A. Monks and J. McMahon *et al*., 1990. New colorimetric cytotoxicity assay for anticancer-drug screening. J. Natl. Cancer Inst., 82: 1107-1112.
32. Allam, R.M., A.M. Al-Abd, A. Khedr, O.A. Sharaf and S.M. Nofal *et al*., 2018. Fingolimod interrupts the cross talk between estrogen metabolism and sphingolipid metabolism within prostate cancer cells. Toxicol. Lett., 291: 77-85.
33. Elagawany, M., A. Abo Elmaaty, A. Mostafa, N.M. Abo Shama, E.Y. Santali, B. Elgendy and A.A. Al-Karmalawy, 2022. Ligand-based design, synthesis, computational insights, and *in vitro* studies of novel *N*-(5-Nitrothiazol-2-yl)-carboxamido derivatives as potent inhibitors of SARS-CoV-2 main protease. J. Enzyme Inhib. Med. Chem., 37: 2112-2132.
34. Gfeller, D., O. Michielin and V. Zoete, 2013. Shaping the interaction landscape of bioactive molecules. Bioinformatics, 29: 3073-3079.
35. Abo Elmaaty, A., W.M. Eldehna, M. Khattab, O. Kutkat and R. Alnajjar *et al*., 2022. Anticoagulants as potential SARS-CoV-2 M^{pro} inhibitors for COVID-19 patients: *In vitro*, molecular docking, molecular dynamics, DFT, and SAR studies. Int. J. Mol. Sci., Vol. 23. 10.3390/ijms232012235.
36. Godschalk, F., S. Genheden, P. Söderhjelm and U. Ryde, 2013. Comparison of MM/GBSA calculations based on explicit and implicit solvent simulations. Phys. Chem. Chem. Phys., 15: 7731-7739.
37. Daina, A., O. Michielin and V. Zoete, 2017. SwissADME: A free web tool to evaluate pharmacokinetics, drug-likeness and medicinal chemistry friendliness of small molecules. Sci. Rep., Vol. 7. 10.1038/srep42717.
38. El-Naggar, A.M., A.M.A. Hassan, E.B. Elkaeed, M.S. Alesawy and A.A. Al-Karmalawy, 2022. Design, synthesis, and SAR studies of novel 4-methoxyphenyl pyrazole and pyrimidine derivatives as potential dual tyrosine kinase inhibitors targeting both EGFR and VEGFR-2. Bioorg. Chem., Vol. 123. 10.1016/j.bioorg.2022.105770.
39. Ghanem, A., A.A. Al-Karmalawy, A.I. Abd El Maksoud, S.M. Hanafy, H.A. Emara, R.M. Saleh and M.F. Elshal, 2022. *Rumex vesicarius* L. extract improves the efficacy of doxorubicin in triple-negative breast cancer through inhibiting Bcl2, mTOR, JNK1 and augmenting p21 expression. Inf. Med. Unlocked, Vol. 29. 10.1016/j.imu.2022.100869.
40. Elebeedy, D., W.F. Elkhatib, A. Kandeil, A. Ghanem and O. Kutkat *et al*., 2021. Anti-SARS-CoV-2 activities of tanshinone IIA, carnosic acid, rosmarinic acid, salvianolic acid, baicalein, and glycyrrhetinic acid between computational and *in vitro* insights. RSC Adv., 11: 29267-29286.
41. El-Demerdash, A., A.A. Al-Karmalawy, T.M. Abdel-Aziz, S.S. Elhady, K.M. Darwish and A.H.E. Hassan, 2021. Investigating the structure-activity relationship of marine natural polyketides as promising SARS-CoV-2 main protease inhibitors. RSC Adv., 11: 31339-31363.
42. El-Megharbel, S.M., S.H. Qahl, B. Albogami and R.Z. Hamza, 2024. Chemical and spectroscopic characterization of (artemisinin/querctin/zinc) novel mixed ligand complex with assessment of its potent high antiviral activity against SARS-CoV-2 and antioxidant capacity against toxicity induced by acrylamide in male rats. PeerJ, Vol. 12. 10.7717/peerj.15638.

43. Mahmoudian, Z.G., A. Ghanbari, I. Rashidi, I. Amiri and A. Komaki, 2023. Minocycline effects on memory and learning impairment in the beta-amyloid-induced Alzheimer's disease model in male rats using behavioral, biochemical, and histological methods. Eur. J. Pharmacol., Vol. 953. 10.1016/j.ejphar.2023.175784.
44. Ohkawa, H., N. Ohishi and K. Yagi, 1979. Assay for lipid peroxides in animal tissues by thiobarbituric acid reaction. Anal. Biochem., 95: 351-358.
45. Marklund, S. and G. Marklund, 1974. Involvement of the superoxide anion radical in the autoxidation of pyrogallol and a convenient assay for superoxide dismutase. Eur. J. Biochem., 47: 469-474.
46. Aebi, H., 1984. Catalase *in vitro*. In: Methods in Enzymology, Packer, L. (Ed.), Academic Press, Cambridge, Massachusetts, United States, ISBN: 9780121820053, pp: 121-126.
47. Hafeman, D.G., R.A. Sunde and W.G. Hoekstra, 1974. Effect of dietary selenium on erythrocyte and liver glutathione peroxidase in the rat. J. Nutr., 104: 580-587.
48. Petrie, A. and C. Sabin, 2009. Medical Statistics at a Glance. 3rd Edn., John Wiley & Sons, Hoboken, New Jersey, ISBN: 9781405180511, Pages: 180.
49. El-Megharbel, S.M. and R.Z. Hamza, 2022. Synthesis, spectroscopic characterizations, conductometric titration and investigation of potent antioxidant activities of gallic acid complexes with Ca(II), Cu(II), Zn(III), Cr(III) and Se(IV) metal ions. J. Mol. Liq., Vol. 358. 10.1016/j.molliq.2022.119196.
50. Nakamoto, K., 1986. Infrared and Raman Spectra of Inorganic and Coordination Compounds. 4th Edn., Wiley, New York, ISBN: 9780471010661, Pages: 496.
51. El-Megharbel, S.M., S.H. Qahl, F.S. Alaryani and R.Z. Hamza, 2022. Synthesis, spectroscopic studies for five new Mg (II), Fe (III), Cu (II), Zn (II) and Se (IV) ceftriaxone antibiotic drug complexes and their possible hepatoprotective and antioxidant capacities. Antibiotics, Vol. 11. 10.3390/antibiotics11050547.
52. Nakamoto, K., 1970. Infrared Spectra of Inorganic and Coordination Compounds. 2nd Edn., Wiley, Hoboken, New Jersey, ISBN: 9780471629801, Pages: 328.
53. Bellamy, L.J., 1975. The Infra-Red Spectra of Complex Molecules. 1st Edn., Springer, Dordrecht, Netherlands, ISBN: 978-94-011-6017-9, Pages: 433.
54. El-Megharbel, S.M., N.M. Al-Baqami, E.H. Al-Thubaiti, S.H. Qahl, B. Albogami and R.Z. Hamza, 2022. Antidiabetic drug sitagliptin with divalent transition metals manganese and cobalt: Synthesis, structure, characterization antibacterial and antioxidative effects in liver tissues. Curr. Issues Mol. Biol., 44: 1810-1827.
55. Garrido-Mesa, N., A. Zarzuelo and J. Gálvez, 2013. What is behind the non-antibiotic properties of minocycline? Pharmacol. Res., 67: 18-30.
56. Klein, N.C. and B.A. Cunha, 1995. Tetracyclines. Med. Clin. North Am., 79: 789-801.
57. Yong, V.W., J. Wells, F. Giuliani, S. Casha, C. Power and L.M. Metz, 2004. The promise of minocycline in neurology. Lancet Neurol., 3: 744-751.
58. Saivin, S. and G. Houin, 1988. Clinical pharmacokinetics of doxycycline and minocycline. Clin. Pharmacokinet., 15: 355-366.
59. Sapadin, A.N. and R. Fleischmajer, 2006. Tetracyclines: Nonantibiotic properties and their clinical implications. J. Am. Acad. Dermatol., 54: 258-265.
60. Kim, H.S. and Y.H. Suh, 2009. Minocycline and neurodegenerative diseases. Behav. Brain Res., 196: 168-179.
61. Amin, A.R., R.N. Patel, G.D. Thakker, C.J. Lowenstein, M.G. Attur and S.B. Abramson, 1997. Post-transcriptional regulation of inducible nitric oxide synthase mRNA in murine macrophages by doxycycline and chemically modified tetracyclines. FEBS Lett., 410: 259-264.
62. Whiteman, M. and B. Halliwell, 1997. Prevention of peroxynitrite-dependent tyrosine nitration and inactivation of α_1-antiproteinase by antibiotics. Free Radical Res., 26: 49-56.
63. Chen, M., V.O. Ona, M. Li, R.J. Ferrante and K.B. Fink *et al*., 2000. Minocycline inhibits caspase-1 and caspase-3 expression and delays mortality in a transgenic mouse model of Huntington disease. Nat. Med., 6: 797-801.
64. Park, J.L. and B.R. Lucchesi, 1999. Mechanisms of myocardial reperfusion injury. Ann. Thoracic Surg., 68: 1905-1912.
65. Webster, G. and J.Q.D. Rosso, 2007. Anti-inflammatory activity of tetracyclines. Dermatologic Clin., 25: 133-135.
66. Miyachi, Y., A. Yoshioka, S. Imamura and Y. Niwa, 1986. Effect of antibiotics on the generation of reactive oxygen species. J. Invest. Dermatol., 86: 449-453.
67. Kraus, R.L., R. Pasieczny, K. Lariosa Willingham, M.S. Turner, A. Jiang and J.W. Trauger, 2005. Antioxidant properties of minocycline: Neuroprotection in an oxidative stress assay and direct radical scavenging activity. J. Neurochem., 94: 819-827.
68. Leite, L.M., A.G.G. Carvalho, P.L.F.T. Ferreira, I.X. Pessoa and D.O. Gonçalves *et al*., 2011. Anti-inflammatory properties of doxycycline and minocycline in experimental models: An *in vivo* and *in vitro* comparative study. Inflammopharmacol, 19: 99-110.
69. Yenari, M.A., L. Xu, X.N. Tang, Y. Qiao and R.G. Giffard, 2006. Microglia potentiate damage to blood-brain barrier constituents: Improvement by minocycline *in vivo* and *in vitro*. Stroke, 37: 1087-1093.
70. Teng, Y.D., H. Choi, R.C. Onario, S. Zhu and F.C. Desilets *et al*., 2004. Minocycline inhibits contusion-triggered mitochondrial cytochrome *c* release and mitigates functional deficits after spinal cord injury. Proc. Natl. Acad. Sci. U.S.A., 101: 3071-3076.

71. Cui, Y., X.X. Liao, W. Liu, R.X. Guo and Z.Z. Wu *et al*., 2008. A novel role of minocycline: Attenuating morphine antinociceptive tolerance by inhibition of p38 MAPK in the activated spinal microglia. Brain Behav. Immunity, 22: 114-123.
72. Al-Salmi, F.A., S.M. El-Megharbel and R.Z. Hamza, 2023. Synthesis and spectroscopic study of novel mixed ligand formula "Artemisinin/Zn" and assessment of its inhibitory effect against "SARS-CoV-2". Heliyon, Vol. 9. 10.1016/j.heliyon.2023.e17177.
73. Hamza, R.Z., F.S. Alaryani, R.E. Alotaibi, M.A. Al-Harthi and G.S. Alotaibi *et al*., 2022. Efficacy of prednisolone/Zn metal complex and artemisinin either alone or in combination on lung functions after excessive exposure to electronic cigarettes aerosol with assessment of antibacterial activity. Crystals, Vol. 12. 10.3390/cryst12070972.
74. Wang, J., Q. Wei, C.Y. Wang, W.D. Hill, D.C. Hess and Z. Dong, 2004. Minocycline up-regulates Bcl-2 and protects against cell death in mitochondria*. J. Biol. Chem., 279: 19948-19954.
75. Castanares, M., Y. Vera, K. Erkkilä, S. Kyttänen and Y. Lue *et al*., 2005. Minocycline up-regulates BCL-2 levels in mitochondria and attenuates male germ cell apoptosis. Biochem. Biophys. Res. Commun., 337: 663-669.
76. Chu, H.C., Y.L. Lin, H.K. Sytwu, S.H. Lin, C.L. Liao and Y.C. Chao, 2005. Effects of minocycline on Fas-mediated fulminant hepatitis in mice. Br. J. Pharmacol., 144: 275-282.
77. Kelly, K.J., T.A. Sutton, N. Weathered, N. Ray, E.J. Caldwell, Z. Plotkin and P.C. Dagher, 2004. Minocycline inhibits apoptosis and inflammation in a rat model of ischemic renal injury. Am. J. Physiol. Renal Physiol., 287: F760-F766.
78. Asadi, A., M. Abdi, E. Kouhsari, P. Panahi and M. Sholeh *et al*., 2020. Minocycline, focus on mechanisms of resistance, antibacterial activity, and clinical effectiveness: Back to the future. J. Global Antimicrob. Resist., 22: 161-174.
79. Hamza, R.Z., Z.A. Sheshah, R.H. Suleman, N.F. Al-Juaid, N.A. Hamed and M.A. Al-Juaid, 2022. Efficacy of some antibiotics and some metal complexes (Nano-formula) that could increase their effectiveness during COVID-19. Int. J. Biol. Pharm. Sci. Arch., 3: 008-014.